AD_____

Award Number: DAMD17-00-1-0517

TITLE: A Quantitative MRI Study of Prostate Cancer Before and After Radiation Therapy

PRINCIPAL INVESTIGATOR: David L. Buckley, Ph.D.

CONTRACTING ORGANIZATION: The University of Manchester
Manchester, United Kingdom
M13 9PT

REPORT DATE: May 2004

TYPE OF REPORT: Final

PREPARED FOR: U.S. Army Medical Research and Materiel Command
Fort Detrick, Maryland 21702-5012

REPORT DOCUMENTATION PAGE

Form Approved
OMB No. 074-0188

1. AGENCY USE ONLY (Leave blank)	2. REPORT DATE	3. REPORT TYPE AND DATES COVERED
	May 2004	Final (15 Apr 2000 - 14 Apr 2004)

4. TITLE AND SUBTITLE
A Quantitative MRI Study of Prostate Cancer Before and After Radiation Therapy

5. FUNDING NUMBERS
DAMD17-00-1-0517

6. AUTHOR(S)
David L. Buckley, Ph.D.

7. PERFORMING ORGANIZATION NAME(S) AND ADDRESS(ES)
The University of Manchester
Manchester, United Kingdom
M13 9PT

E-Mail: david.buckley@man.ac.uk

8. PERFORMING ORGANIZATION REPORT NUMBER

9. SPONSORING / MONITORING AGENCY NAME(S) AND ADDRESS(ES)
U.S. Army Medical Research and Materiel Command
Fort Detrick, Maryland 21702-5012

10. SPONSORING / MONITORING AGENCY REPORT NUMBER

11. SUPPLEMENTARY NOTES

12a. DISTRIBUTION / AVAILABILITY STATEMENT
Approved for Public Release; Distribution Unlimited

12b. DISTRIBUTION CODE

13. ABSTRACT (Maximum 200 Words)

The purpose of the study was to examine the influence of external beam radiation on the prostate and prostate cancer using novel quantitative MRI techniques. Twenty-two men, previously diagnosed with prostate cancer, were studied using T1 and T2 relaxation mapping and contrast agent kinetic methods before and after treatment by radiotherapy. The MRI findings will be correlated with biochemical (prostate specific antigen) progression and biopsy results.

All 22 patients have been recruited and studied pre-treatment. So far nineteen patients have returned for follow-up MRI. The data is both complete and of a high quality. Data analysis of the pre-treatment phase has provided important and novel information about the microvascular characteristics of prostate cancer. These results have been accepted for publication in the leading radiology journal. Preliminary analysis of the post-treatment data is promising and awaits clinical interpretation.

14. SUBJECT TERMS
Magnetic resonance imaging, contrast agents, radiation therapy, angiogenesis, biological modeling

15. NUMBER OF PAGES
40

16. PRICE CODE

17. SECURITY CLASSIFICATION OF REPORT	18. SECURITY CLASSIFICATION OF THIS PAGE	19. SECURITY CLASSIFICATION OF ABSTRACT	20. LIMITATION OF ABSTRACT
Unclassified	Unclassified	Unclassified	Unlimited

Table of Contents

INTRODUCTION

Prostate cancer is already the most common malignancy in men, and with an ever-aging population the incidence of the disease is certain to increase. Surgery is the most common form of treatment for localized disease but many thousands of patients undergo radiation therapy each year in the United States. The advent of PSA testing and an increasing public awareness of the disease suggest that more and more patients will select radiation treatment to avoid the potential side effects of surgery. The use of radiation therapy is not definitive, and with between 30 and 70% of patients suffering an increasing PSA 5 years after treatment, improved methods of patient follow-up are needed.

Magnetic resonance imaging (MRI) offers the most accurate staging information when cancer is confined to the gland. However, only one study to date has looked at patients following radiation treatment and the findings were inconclusive. A preliminary prospective, quantitative study, such as this, is an essential step in the assessment of MRI of the irradiated gland. The information obtained from such a study will provide important physiological and structural information about the prostate gland and the changes induced by treatment. These changes have implications, not only for MR interpretation, but also for pathological analysis of biopsy specimens.

The following report details the final results of a quantitative magnetic resonance imaging (MRI) study of prostate cancer before and after radiation therapy. The study aimed to examine the influence of external beam radiation on the prostate and prostate cancer using novel quantitative MRI techniques. Twenty-two men, previously diagnosed with prostate cancer, were studied using T1 and T2 magnetic resonance relaxation mapping and contrast agent kinetic methods before and after treatment by radiotherapy. The MRI findings will be correlated with biochemical (prostate specific antigen) and biopsy results.

BODY

The following section summarises the research accomplishments associated with the tasks outlined in the approved Statement of Work. Despite the delays experienced in transferring the grant funding from the University of Florida to the University of Manchester and the subsequent delay in obtaining Human Subjects approval (detailed in the Year 1 annual report), significant progress has been made with the Statement of Work. The research accomplishments associated with each of the tasks outlined are described below.

Task 1.

Months 1-6. To complete the imaging sequence design and testing. (specific aims 1 and 2).

a. The T1/T2 phantom will be constructed.
b. Calibration of the dynamic imaging sequences (proton density weighted + T1-weighted sequences)
c. Optimization of the FSE, T2 imaging sequence.
d. Selection of dynamic and T2 imaging sequences. Finalize imaging protocol.

As noted in the Year 1 report, with the cooperation of Drs. Steve Blackband, Amanda Barry (Post-Doctoral Research Assistant employed during the first year of the study) and Geoff Parker (Research Fellow working on related studies), all elements of *Task 1* were successfully completed.

Task 2.

Months 7-12. Dynamic data simulation and model development (specific aim 1). Software development (specific aims 1 and 2).

a. Compare simulated data with patient data (both existing and data being acquired in task 3).
b. Error propagation analysis of models under test.
c. Software development. T2 maps and dynamic data analysis.

a. &
b. All elements of *Task 2* were completed (as outlined in the Year 2 and Year 3 annual reports) but this work continues to provide the stimulus for further related developments. In particular, the analysis of errors in the techniques employed has led to further work on the assessment of dynamic T1 measurement. The positive findings of this work stress the importance of arterial input function assessment for minimising measurement errors. Such measurements are made in this study:

    i. Appendix 1. An abstract entitled, "T1 estimation using variable flip angle spoiled gradient echo for dynamic contrast-enhanced MRI: Arterial input measurement improves accuracy in the presence of B1 error" was accepted for presentation at the 12th Annual Meeting of the International Society for Magnetic Resonance in Medicine (Kyoto, May 2004). The abstract describes errors associated with contrast agent measurements and how these may be minimised by data analysis employing concurrent measurement of the arterial input function.

c. Software for the analysis of the MR data is in place and has been used in the subsequent tasks. Examples of the results obtained were presented in the Year 2 report (Figures 1, 2 and 3).

Task 3.

Months 7-18. Patient recruitment (21 patients) and examination for pretreatment phase of specific aim 3.

a. In collaboration with Pathology, examine recent biopsy data for potential patients.
b. Select patients (in collaboration with Mr. Clarke) for the study. Obtain written, informed consent.
c. Acquire data from the 1.5 T system. Backup (optical disks) and transfer data to laboratory.
d. Stain and reanalyze biopsy specimens.

---

a. &
b. A total of 22 patients were successfully identified, recruited and consented by the end of February 2003. A further suitable patient was included in the study after writing of the 2003 annual report.
c. Data were successfully acquired from all patients. Ten patients (described in the Year 2 report) were scanned between July 2001 and March 2002; the remaining 12 patients were scanned between May 2002 and March 2003. All data were backed-up on both optical disk and CD.
d. As noted in the Year 2 and Year 3 reports, it had been decided that the most efficient and appropriate means of analysing the biopsy specimens was to process them as a batch. However, it has since become apparent that we may receive fewer samples than originally expected thus work is now underway, by Drs. West and Clarke, to assess the possibility of analysing pre-treatment samples obtained from various outlying hospitals (the original referring sites).

Task 4.

Months 13-24. Data analysis, pretreatment phase.

a. Generation of Gd-DTPA concentration maps, uptake rate/max uptake maps and T2 maps.
b. Image review with biopsy results. Preliminary identification of cancer/BPH/normal tissue.
c. Region of interest analysis. Model fitting (dynamic data).

---

a. As noted in the Year 3 report, maps were generated for each patient. Examples of these were presented in the Year 2 report (Figs. 1, 2 and 3).
b. As noted in the Year 3 report, Dr. Charles Hutchinson, with the help of Mr. Roberts and Dr. Buckley, identified regions of suspected tumour, normal peripheral zone and muscle (internal obturator, chosen as a reference tissue). A total of 22 tumour and 22 muscle regions were defined in 22 patients. Normal-appearing peripheral zone was not visible in two patients thus only 20 normal prostate regions were defined.
c. As noted in last year's report, these data were all analysed successfully. The results were subsequently presented at the 11th Annual Meeting of the International Society for Magnetic Resonance in Medicine (Toronto, July 2003):

i. Appendix 2. An abstract entitled, "*In vivo* determination of the microvascular characteristics of prostate cancer using dynamic contrast-enhanced MRI" was presented, in an oral clinical science focus session at the 11th Annual Meeting of the International Society for Magnetic Resonance in Medicine (Toronto, July 2003). The abstract (written in November 2002) details only the first few patients studied but the entire 22-patient data set was presented at the meeting.

These data have now been fully analysed and the results are described in a manuscript that has been accepted for publication by the journal *Radiology*, the leading publication (highest impact factor) in this field [1]. Full details of these results are presented in the attached manuscript (Appendix 3):

ii. Appendix 3. A full paper, "Vascular characteristics of prostate cancer: Evaluation with dynamic contrast-enhanced T1-weighted MRI – initial experience" *in press* in the journal *Radiology* (accepted for publication April 29th, 2004).

In addition to the vascular data, the relaxation data were also fully analysed. These results (combined with the complete vascular data set) are shortly to be presented at the 12th Annual Meeting of the International Society for Magnetic Resonance in Medicine (Kyoto, May 2004). The results are detailed in the abstract:

i. Appendix 4. An abstract entitled, "Characterization of prostate cancer by quantitative MRI" accepted for oral presentation at the 12th Annual Meeting of the International Society for Magnetic Resonance in Medicine (Kyoto, May 2004). The abstract describes the complete quantitative data set from the pre-treatment prostates.

Task 5.

Months 19-30. Patient follow-up (21 patients) and examination for post-treatment phase of specific aim 3.

a. Request 2nd examination for each of the patients studied in task 3.
b. Acquire data from the 1.5 T system. Backup (optical disks) and transfer data to laboratory.

a. &
b. To date 19 patients have undergone their follow-up MR examinations and, as previously, all their data was backed-up to both optical disk and CD. The mean follow-up time was 14 months post-radiotherapy (range 12 to 17 months). Two further patients are due follow-up MR in May and July of 2004. One patient developed metastases and, due to their illness, was unable to undergo follow-up MR. This patient has since died. Dr. Logue and his staff continue to coordinate the follow-up of all patients.

Task 6.

Months 19-30. Data analysis, post-treatment phase.

a. Generation of Gd-DTPA concentration maps, uptake rate/max uptake maps and T2 maps.
b. Image review with previous MRI and biopsy results. Identification of cancer/BPH/normal tissue.
c. Region of interest analysis. Model fitting (dynamic data).

a. Relaxation rate maps have been generated for 19 patients while tracer kinetics analysis is complete on 12 patients.
b. The task of identifying cancer and normal tissue is complicated by the tissue changes caused by radiotherapy. These include generalised loss of signal from the prostate gland and, in particular, a loss of internal structural contrast. Dr. Charles Hutchinson has in some cases identified regions of suspected residual tumour while in others has simply drawn new regions to match as closely as possible to the regions drawn on the pre-treatment images. A similar approach has been taken for the normal peripheral zone. Muscle regions have also been identified.
c. Relaxation data from 19 patients has been analysed successfully. The results are outlined in the figure below. It is currently too early to speculate on the significance of the tracer kinetics analysis

(with only 12 complete data sets analysed to date) and a full analysis will be postponed until the follow-up study is complete.

Figure 1.
Relaxation data (T1 and T2) measured in regions of tumour, normal prostate gland and muscle. Data are shown for 19 patients examined before and 14 months after radiotherapy. Significant increases following radiotherapy are seen in tumour T1 and muscle T2 ($p < 0.01$, paired t-test) and a small decrease is seen in normal prostate gland T2 ($p < 0.05$).

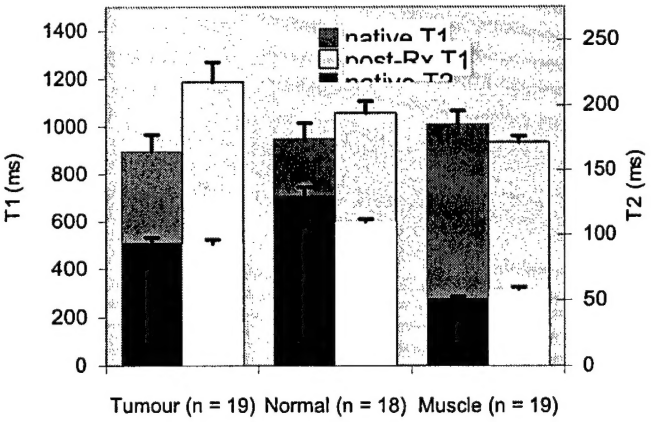

Task 7.

Months 31-36. Review of results, patient follow-up and publication.

a. Obtain follow-up biopsies on each patient (18 months after treatment).
b. Stain and analyze biopsy specimens.
c. Review each patients clinical and biochemical data.
d. Compare and correlate MRI data and clinical data.
e. Publication of significant findings/experience.

a. To date follow-up biopsies have been requested for 12 patients. Three patients declined to undergo the procedure and four patients have relapsed and have selected further treatment such that biopsy was not recommended. Thus only five patients have undergone follow-up biopsy.
b. Dr. West has recently taken samples from the five follow-up biopsies and is assessing them for CD31/CD34 antibody staining.
c. Dr. Logue and his team continue to review the patients studied. We have complete records of all biochemical tests (PSA) and the patients are now being stratified into responders and non-responders. We anticipate this assessment will be completed by the summer.
d. The comparison of histopathology, clinical findings and MR data is now underway. The pre-treatment MR data will be compared with post-treatment using patient response (determined by analysis of PSA levels) as a covariate. These data will be reported in the literature as soon as they have been fully analysed and interpreted.
e. Two full papers have been produced from the data accrued and analysed thus far (one published [2], Appendix 5; one accepted for publication [1], Appendix 3). It is anticipated that *at least* two further papers will be submitted to leading journals to describe the findings of the post-treatment data. One to illustrate the changes in prostate physiology in response to radiotherapy and one to assess the prognostic capabilities of contrast-enhanced MRI in this patient group.

KEY RESEARCH ACCOMPLISHMENTS

- Implementation of a quantitative imaging protocol suitable for analysis with a distributed parameter tracer kinetics model (i.e. rapid data acquisition with arterial input measurement).
- Acquisition of data from 22 patients pre-treatment. The data has been fully analysed, assessed and published in a leading journal.
- Complete follow-up data obtained in 19 patients.

- Preliminary analysis of relaxation data indicates excellent data quality and post-radiotherapy changes in both prostate and nearby muscle.

REPORTABLE OUTCOMES:

The outcomes are listed in chronological order:

1. July 2003.
Abstract. G.J. Parker, A. Jackson, J.C. Waterton, D.L. Buckley, "Automated arterial input function extraction for T1-weighted DCE-MRI", presented at the 11th Annual Meeting of the International Society for Magnetic Resonance in Medicine (Toronto, Canada).

2. July 2003.
Abstract. D.L. Buckley, C. Roberts, G.J. Parker, J.P. Logue, C.E. Hutchinson, "*In vivo* determination of the microvascular characteristics of prostate cancer using dynamic contrast-enhanced MRI", presented at the 11th Annual Meeting of the International Society for Magnetic Resonance in Medicine (Toronto, Canada).

3. February 2004.
Abstract. D.L. Buckley, G.J.M. Parker, "T1 estimation using variable flip angle spoiled gradient echo for dynamic contrast-enhanced MRI: Arterial input measurement improves accuracy in the presence of B1 error" accepted for presentation at the 12th Annual Meeting of the International Society for Magnetic Resonance in Medicine (Kyoto, May 2004).

4. February 2004.
Abstract. D.L. Buckley, C. Roberts, S.K. Khaki, G.J.M. Parker, J.P. Logue, C.E. Hutchinson, "Characterization of prostate cancer by quantitative MRI" accepted for oral presentation at the 12th Annual Meeting of the International Society for Magnetic Resonance in Medicine (Kyoto, May 2004).

5. April 2004.
Paper. D.L. Buckley, C. Roberts, G.J.M. Parker, J.P. Logue, C.E. Hutchinson "Vascular characteristics of prostate cancer: Evaluation with dynamic contrast-enhanced T1-weighted MRI – initial experience" accepted for publication by the journal *Radiology*.

CONCLUSIONS

The study is nearing completion with excellent results obtained for almost all aspects of the work. All patients have been studied successfully prior to radiotherapy and these data form the basis of a manuscript recently accepted for publication in the leading journal, *Radiology* [1]. These results are both novel and world leading, being the first such reported measurements using MRI. Recent reports in the literature highlight the developing interest in this field of MRI [3,4] and another CT study adopts a similar approach, though without the specificity of MRI [5]. In combination with the vascular physiology, MR relaxation measurements match well to previously reported results [6]. All that remains to be assessed in the pre-treatment phase is the biopsy data, and the effort to obtain these data is on going.

The follow-up phase of the study is almost complete. Only one patient was unable to complete the study having developed metastases. Preliminary analysis of the relaxation measurements highlights the quality of the data and indicates a number of tissue changes 14 months after radiotherapy. We anticipate further insight once the clinical data is fully interpreted and the patients are stratified into responders and non-responders. At this point the prognostic capabilities of the MRI techniques will be tested. In summary, the study, despite some initial delays, has been a resounding success. There remains work to be done but we anticipate future studies to build upon these successes.

REFERENCES

1. D.L. Buckley, C. Roberts, G.J.M. Parker, J.P. Logue, C.E. Hutchinson, Vascular characteristics of prostate cancer: Evaluation with dynamic contrast-enhanced T1-weighted MRI – initial experience. Radiology 2004; in press.
2. Buckley DL. Uncertainty in the analysis of tracer kinetics using dynamic contrast-enhanced T1-weighted MRI. Magn Reson Med 2002;47:601-606
3. Engelbrecht MR, Huisman HJ, Laheij RJF, et al. Discrimination of prostate cancer from normal peripheral zone and central gland tissue by using dynamic contrast-enhanced MR imaging. Radiology 2003; 229:248-254.
4. Schlemmer HP, Merkle J, Grobholz R, et al. Can pre-operative contrast-enhanced dynamic MR imaging for prostate cancer predict microvessel density in prostatectomy specimens? Eur. Radiol. 2004; 14:309-317.
5. Henderson E, Milosevic MF, Haider MA, Yeung IWT. Functional CT imaging of prostate cancer. Phys. Med. Biol. 2003; 48:3085-3100.
6. Liney, G. P., Turnbull, L. W., Lowry, M., Turnbull, L. S., Knowles, A. J. and Horsman, A. In vivo quantification of citrate concentration and water T2 relaxation time of the pathologic prostate gland using H-1 MRS and MRI. Magn Reson Imaging 1997; 15:1177-1186.

BIBLIOGRAPHY

1. September 2000:
Abstract. D.L. Buckley, "Uncertainty in the measurement and analysis of tracer kinetics using dynamic contrast-enhanced MRI", presented at the European Society for Magnetic Resonance in Medicine and Biology (ESMRMB) 17th Annual Meeting and published in the journal *MAGMA*, **11**, 123-124, 2000.

2. February 2002.
Letter. D.L. Buckley, "Transcytolemmal water exchange and its affect on the determination of contrast agent concentration *in vivo*", published as a Letter to the Editor by *Magnetic Resonance in Medicine,* volume 47, pages 420-421, 2002

3. March 2002.
Paper, D.L. Buckley, "Uncertainty in the analysis of tracer kinetics using dynamic contrast-enhanced T1-weighted MRI", published in the journal *Magnetic Resonance in Medicine*, volume 47, pages 601-606, 2002.

4. May 2002.
Abstract. D.L. Buckley, "The influence of transcapillary water exchange on the analysis of tracer kinetics in dynamic Gd-DTPA-enhanced T1-weighted MRI", presented at the International Society for Magnetic Resonance in Medicine (ISMRM) 10th Annual Meeting.

5. July 2003.
Abstract. G.J. Parker, A. Jackson, J.C. Waterton, D.L. Buckley, "Automated arterial input function extraction for T1-weighted DCE-MRI", presented at the 11th Annual Meeting of the International Society for Magnetic Resonance in Medicine.

6. July 2003.
Abstract. D.L. Buckley, C. Roberts, G.J. Parker, J.P. Logue, C.E. Hutchinson, "*In vivo* determination of the microvascular characteristics of prostate cancer using dynamic contrast-enhanced MRI", presented at the 11th Annual Meeting of the International Society for Magnetic Resonance in Medicine.

7. April 2004.
Paper. D.L. Buckley, C. Roberts, G.J.M. Parker, J.P. Logue, C.E. Hutchinson "Vascular characteristics of prostate cancer: Evaluation with dynamic contrast-enhanced T1-weighted MRI – initial experience" accepted for publication by the journal *Radiology*.

PERSONNEL

David L. Buckley; Amanda Barry; Caleb Roberts; Geoffrey Parker; Stephen J. Blackband; John Logue; Noel Clarke; Catharine West

T_1 estimation using variable flip angle spoiled gradient echo for dynamic contrast-enhanced MRI: Arterial input measurement improves accuracy in the presence of B_1 error

D. L. Buckley[1], G. J. Parker[1]

[1]Imaging Science and Biomedical Engineering, University of Manchester, Manchester, United Kingdom

Introduction.

An essential step in the quantitative analysis of contrast agent uptake is the assessment of changes in tissue T_1. The rapid acquisition times often required for these measurements dictate that they are made using gradient echo pulse sequences with flip angles < 90°. Quantitative measurements made using such sequences rely on accurate knowledge of B_1 and it is well known that many transmit coils can produce inhomogeneous B_1 fields and this can be compounded by slice profile and dielectric resonance effects [1,2]. In this study, the effect of a systematic error in B_1 on the measurement of contrast agent uptake in tissues is examined.

Methods.

For these simulations input data ($1/T_1$ against time) were taken from regions encompassing a prostate tumour, normal peripheral zone and an external iliac artery (to provide an arterial input function, AIF) following the administration of 0.1 mmol/kg Gd-DTPA-BMA. The original data were acquired on a 1.5 T Philips MR system every 2.3 s for 4 minutes using a 3D T_1-weighted gradient echo pulse sequence with a TR of 2.5 ms and a flip angle of 30° [3]. Baseline T_1 had been estimated using 4 acquisitions at 2°, 10°, 20° and 30° flip angles [4]. From the temporal changes in $1/T_1$ signal intensity time courses were simulated for a series of acquisitions with ±10% and ±30% errors in B_1. That is, for acquisitions with true flip angles of 21°, 27°, 33° and 39° instead of the nominal 30°. These errors applied equally to the data used for baseline T_1 estimates (e.g. a -10% error in the flip angle will result in acquisitions at 1.8°, 9°, 18° and 27° instead of the nominal 2°, 10°, 20° and 30°). The data resulting from these simulations were subsequently converted to temporal changes in $1/T_1$ (using the erroneous assumption of correct flip angles) and analyzed using a two-compartment model providing estimates of K^{trans}, v_e and v_b [5]. Two analyses were performed: 1. By assuming an independently measured AIF (errors in the flip angle do not affect the AIF and it remains in its original form), 2. By assuming the AIF is measured by the same method used to image the tissue (errors in the flip angle affect the AIF and tissue equally).

Results.

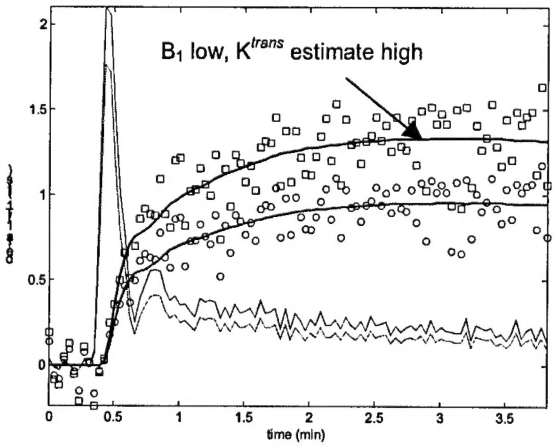

Fig. 1 True $1/T_1$ time course in an artery (faint red line, scaled down by a factor of 10) and normal prostate (circles with model fit in red). Estimated $1/T_1$ time course in artery (faint blue line) and prostate (squares with model fit in blue) when flip angle error = -30%.

The true baseline T_1 of the prostate and artery was 1000 ms and 1500 ms, respectively. A -30% error in the flip angle results in baseline T_1 estimates of 486 ms and 728 ms, respectively, and an overestimate in the amplitude of the $1/T_1$ time courses. Positive errors in the flip angles led to overestimates of T_1 (up to 1713 ms for the prostate) and concomitant underestimates in the amplitude of the $1/T_1$ time courses. When the simulated data were presented for fitting by method 1 errors in K^{trans}, v_e and v_b were of the same magnitude and ranged from -24% to +40% (resulting from +30% to -30% flip angle errors). When presented for fitting by method 2 errors in K^{trans} ranged from -3% to +10%; errors in v_e ranged from -3% to +1% and errors in v_b ranged from -6% to +21%.

Discussion.

Systematic errors in the amplitude of flip angles are common in the clinical setting [6]. Correction of the ensuing errors can be accomplished by careful system calibration [2,6] but this may be impractical in many situations. When encountered in dynamic contrast-enhanced studies corrections can be made using a bookend T_1 measurement approach [7]. However, this requires accurate baseline and post-contrast T_1 measurements that are insensitive to B_1 errors. When left uncorrected errors propagate into the estimates of $1/T_1$ (Fig. 1) and thereby into estimates of contrast agent concentration. When the data are later analysed using a tracer kinetic model the parameter estimates will be inaccurate. Errors in K^{trans} of 40% result from a -30% error in B_1. These errors are magnified as TR increases or the nominal flip angle used for the dynamic acquisition decreases. However, if measurements of the AIF and tissue residue curve are made simultaneously then subsequently used for tracer kinetic analysis, errors in the resultant parameter estimates are significantly reduced. Hence a -30% error in B_1 results in only a 10% error in K^{trans}. This improvement arises since the B_1 miscalculation affects the AIF and tissue $1/T_1$ to a similar degree. Hence the use of a measured AIF not only improves the underlying accuracy of parameter estimates [5] but also reduces sensitivity to B_1 error.

Acknowledgments. Funded by the U.S. Department of Defense Prostate Cancer Research Program (PC991154).

References. **1.** Alecci M et al. *Magn Reson Med* 46:379-85 (2001). **2.** Parker GJ et al. *Magn Reson Med* 45:838-45 (2001); **3.** Buckley DL et al. *Proc 11th meeting ISMRM*, Toronto, 461 (2003); **4.** Zhu XP et al. *J Magn Reson Imaging* 11:575-585 (2000); **5.** Buckley DL *Magn Reson Med* 47:601-606 (2002); **6.** Brookes JA et al. *J Magn Reson Imaging* 9:163-171 (1999); **7.** Cron GO et al. *Magn Reson Med* 42:746-753 (1999).

In vivo determination of the microvascular characteristics of prostate cancer using dynamic contrast-enhanced MRI

D. L. Buckley[1], C. Roberts[1], G. J. Parker[1], J. P. Logue[2], C. E. Hutchinson[1]

[1]University of Manchester, Imaging Science & Biomedical Engineering, Manchester, England, United Kingdom, [2]Department of Clinical Oncology, Christie Hospital, Manchester, England, United Kingdom

Synopsis.
Tumour angiogenesis is a recognised prognostic indicator in patients with prostate cancer treated with external beam radiotherapy. Using rapid dynamic contrast-enhanced 3D MRI and a distributed parameter tracer kinetic model the microvascular characteristics of prostate cancer were assessed in a group of patients prior to treatment with radiotherapy. Blood flow was higher in the tumours than in normal peripheral zone but there were no significant differences in PS product or blood volume. This novel approach may prove valuable as a prognostic tool and the patients will be studied post-treatment to assess tissue response.

Introduction.
Baseline estimates of blood flow and capillary permeability are required to assess response of the prostate to treatment. The purpose of this study was to assess the microvascular characteristics of the pathological prostate gland prior to treatment with external beam radiotherapy using dynamic contrast-enhanced MRI and a distributed parameter tracer kinetic model [1]. The hypothesis to be tested is that these characteristics will be sensitive indicators of tissue response to treatment and thereby provide a useful prognostic tool.

Methods.
After obtaining written informed consent, data were acquired from 15 patients with biopsy confirmed stage T2 or T3 carcinoma of the prostate gland. These patients all selected external beam radiotherapy for subsequent treatment of their disease. The patients were scanned on a 1.5 T Philips MR system using a pelvic phased-array coil and a 3D T_1-weighted gradient echo pulse sequence. Images were acquired using flip angles of 2°, 10°, 20° and 30° to estimate baseline T_1 [2]. This was followed by a dynamic series in which volumes (flip angle 30°) were acquired every 2.3 s for approximately 4 minutes. Early in this series 0.1 mmol/kg Gd-DTPA-BMA was injected at 3 ml/s using a power injector.

The image data were subsequently analysed off-line. For each patient regions of interest were drawn in the external iliac or femoral arteries (to provide a vascular input function). With the aid of T_2-weighted images a radiologist (CEH) drew further regions in prostate tumour, muscle (internal obturator) and, where possible, normal contralateral peripheral zone. Signal intensity variations in these regions were converted to temporal changes in Gd-DTPA-BMA concentration [2] and a distributed parameter model [1] was fitted to the data. Parameters estimates in each region were compared using a paired t-test.

Results.
Analysis of the data from each region provided estimates (mean ± SD) of blood flow (F), blood volume (V_b) and microvascular permeability-surface area product (PS) [3].

Tissue	F (ml/100 ml/min)	V_b (ml/100 ml)	PS (ml/100 ml/min)
Tumour (n=14)	81 ± 66	2.1 ± 3.7	24 ± 11
Normal (n=12)	30 ± 16	1.6 ± 2.6	15 ± 12

Discussion.
These findings highlight the capabilities of MR imaging to estimate parameters only previously measured using PET [4] or CT [5]. The preliminary results confirm that blood flow to tumour tissue exceeds that to normal prostatic tissue ($p = 0.02$) [4] but suggests that blood volume and capillary permeability may not be significantly different ($p = 0.51$ and 0.37, respectively). In line with previous MR studies [6,7], K^{trans} was significantly higher in tumour than normal peripheral zone ($p<0.0005$). Further studies are ongoing and the patients will all be rescanned 12 months after treatment. These initial findings show considerable promise for isolating the physiological basis for contrast enhancement in the prostate.

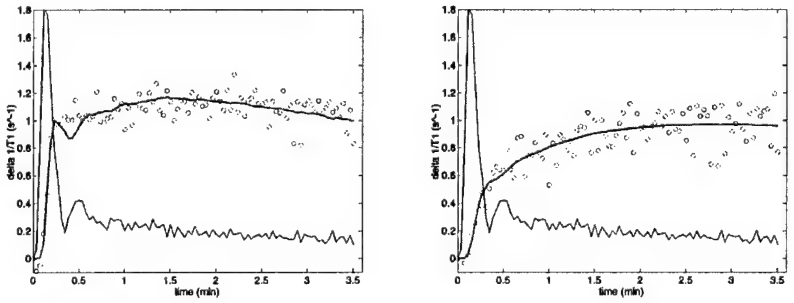

Figure 1. Changes in $1/T_1$ measured over time in tumour (left) and normal peripheral zone (right) of the same patient. Blue lines show the vascular input function (scaled down by a factor of 10) measured in the external iliac artery and the red lines represent model fits to the data.

Acknowledgments. Funded by the U.S. Dept. of Defense Prostate Cancer Research Program (PC991154). Jeanette Lyons, Yvonne Watson and David Clark kindly helped with the patient studies.

References

1. St. Lawrence KS, Lee TY *J Cereb Blood Flow Metab* 18:1365-1377 (1998); **2.** Zhu XP et al. *J Magn Reson Imaging* 11:575-585 (2000); **3.** Buckley DL *Magn Reson Med* 47:601-606 (2002); **4.** Inaba T *J Urol* 148:1457-1460 (1992); **5.** Koh TS et al. *Phys Med Biol* 46:1519-1538 (2001); **6.** Turnbull LW et al. *J Magn Reson Imaging* 9:311-316 (1999); **7.** Padhani AR et al. *Clin Radiol* 55:99-109 (2000)

Accepted for publication by *Radiology* – April 2004

Vascular characteristics of prostate cancer: Evaluation with dynamic contrast-enhanced T_1-weighted MRI – initial experience

David L. Buckley[1], Ph.D.

Caleb Roberts[1], B.Sc.

Geoff J.M. Parker[1], Ph.D.

John P. Logue[2], MB ChB, FRCR

Charles E. Hutchinson[1], MD, FRCR

1. Imaging Science and Biomedical Engineering, University of Manchester, Manchester, United Kingdom.

2. Department of Clinical Oncology, Christie Hospital, Manchester, United Kingdom.

Abbreviated title: Vascular characteristics of prostate cancer

Address for correspondence:

David L. Buckley, Ph.D.
Imaging Science and Biomedical Engineering
University of Manchester
Stopford Building, Oxford Road
Manchester M13 9PT
United Kingdom
Tel. ++44 161 275 5759
Fax. ++44 161 275 5145
E-mail: david.buckley@man.ac.uk

Grant support: This work was supported by a grant from the U.S. Department of Defense Prostate Cancer Research Program (PC991154).

Submission category: *Original Research*

Abstract

PURPOSE: To use contrast-enhanced magnetic resonance imaging (MRI) and a distributed parameter tracer kinetics model prospectively for evaluation of vascular characteristics of prostate cancer.

MATERIALS AND METHODS: Twenty-two patients aged between 57 and 76 years old (mean, 67 years) with histologically proven adenocarcinoma of the prostate were studied at 1.5 T using 3D dynamic contrast-enhanced T_1-weighted MRI. Data from regions of interest drawn in tumor, normal-appearing peripheral zone tissue and muscle were analyzed to provide estimates of perfusion, blood volume, interstitial volume and microvascular permeability-surface area product. These estimates were compared using non-parametric Wilcoxon Signed Ranks test.

RESULTS: Blood flow in prostate tumors (n=22; mean, 66 ml/100 ml/min) was significantly higher than in contralateral peripheral zone (n=20; 32 ml/100 ml/min). Similarly the interstitial distribution volume in tumors was enlarged (42 ml/100 ml in tumor versus 27 ml/100 ml in normal peripheral zone). Blood volume and microvascular permeability-surface area product in tumors (1.0 ml/100 ml and 22 ml/100 ml/min, respectively) were indistinguishable from values estimated in peripheral zone tissue (1.5 ml/100 ml and 21 ml/100 ml/min, respectively).

CONCLUSION: These findings show considerable promise for isolating vascular characteristics of prostate cancer.

Keywords: magnetic resonance (MR), tissue characterization; prostate neoplasms; neoplasms, blood supply.

Introduction

Magnetic resonance imaging (MRI) remains the most promising technique for the detection and staging of prostate cancer despite its current limitations in sensitivity and specificity [1]. Conventional MRI, typically by means of fast T_2-weighted spin echo acquisitions, provides excellent anatomical images of the gland in which the normal peripheral zone and central gland may be distinguished. However, malignant tissue is not always clearly visualized particularly when it co-exists with benign prostatic hyperplasia (BPH) in the central gland [2]. Although initially considered to be of limited use for studying the prostate [3], contrast-enhanced MRI has shown promise in a series of studies employing rapidly acquired early or dynamic data post-contrast administration [4-7]. In these studies, cancers (principally in the peripheral zone of the gland) are seen to enhance more rapidly [5] or avidly [7] than normal tissues.

It is likely that the early enhancement seen in cancer is due, in part, to angiogenesis associated with early tumor growth. The growth of prostate cancer is associated with the development of a rich blood supply fed by a large network of immature, leaky blood vessels [8]. The density of this network is related to tumor grade and metastatic potential [9]. Since conventional methods of assessing angiogenesis require the processing of pathological specimens there is considerable interest in developing non-invasive tools to assess the microvascular characteristics of prostate cancer *in vivo* [10]. A link between contrast uptake in solid tumors and their microvascular characteristics certainly exists but the precise relationship between the tracer kinetics measured, often in terms of heuristic measures, and the microvessel density measured pathologically remains unclear [11, 12]. The assessment of tracer kinetics in absolute physiological terms may help to address this question [13]. Increasing microvessel density will lead to an increase in blood flow, blood volume and the surface area of vessel walls. An upturn in vascular endothelial growth factor production is likely to increase the permeability of these vessel walls. Blood flow, blood volume and microvascular permeability-surface area product are all, in principle, quantifiable through the

analysis of contrast-enhanced imaging data using distributed parameter tracer kinetics models [10, 14]. These have yet to be applied *in vivo* to a meaningful patient group using MRI, though a recent preliminary X-ray computerized tomography (CT) study has shown promising results [15].

The use of tracer kinetics modeling in the analysis of tomographic images of the prostate is widespread; from the earliest positron emission tomography (PET) study [16], through a series of MRI [17-19] and CT studies [15, 20]. While the MRI studies have provided sufficient spatial and contrast resolution to identify cancer, normal peripheral zone and BPH within individual glands, there is limited information about the microvascular characteristics of these tissues. Studies employing compartmental models have shown that peripheral zone cancers have higher extraction-flow products (K^{trans}, [21]) than normal peripheral zone tissue [17, 18]. This finding is supported by the generally higher blood flow measured in tumor-bearing prostates compared to those containing BPH alone [16]. Differences between tumors and normal, BPH-containing, tissue in the central gland are less clear-cut though a recent MRI study highlighted potential differences in flow-related parameters [22]. Thus, the purpose of our study was to use contrast-enhanced MRI and a distributed parameter tracer kinetics model prospectively for evaluation of vascular characteristics of prostate cancer.

Materials and Methods

Tracer kinetic model

There are distinct advantages to employing a distributed parameter model for analysis of tracer kinetics [23]. By definition compartmental models disregard the tracer's microvascular transit time and it is assumed to be negligible on the time scale of typical T_1-weighted MRI acquisitions. Once the temporal resolution of the experiment is comparable to the transit time, the use of a distributed parameter model becomes a realistic option [24]. Johnson and Wilson introduced a simple distributed parameter model in which the internal capillary space contains a tracer, the concentration of which varies in both time and space (along the capillary length) [25]. Tracer in the capillary space is in exchange with an external interstitial space that behaves as a well-mixed compartment (i.e. there is no spatial variation in tracer concentration). St. Lawrence and Lee introduced an adiabatic approximation to this model in 1998 providing a time-domain solution suitable for the analysis of imaging data [24]:

$$C_{tis}(t) = F\int_0^{\tau} C_b(t-u)du + EF\int_{\tau}^{t} C_b(u)\exp\left(\frac{-EF(1-hct)}{V_e}(t-u-\tau)\right)du \qquad (1)$$

where C_{tis} and C_b are the concentrations of contrast agent over time, t, in the tissue of interest and blood, respectively. F is the tissue blood flow, hct is the blood hematocrit and τ is the mean microvascular transit time equal to the blood volume, V_b, divided by F. V_e is the interstitial tracer distribution volume, u is a dummy integration variable and the extraction fraction, E = 1 – exp(-PS/F(1-hct)) where PS is the microvascular permeability-surface area product. The product EF(1-hct) is also referred to as K^{trans} [21]. This model contains 4 unknown parameters that may be estimated by curve fitting: F, E, V_e and τ. From these, the parameters PS and V_b may be evaluated. This model has since been used successfully for the analysis of both MRI and CT data [15, 26, 27].

Patients

Twenty-two consecutive men with histologically proven adenocarcinoma of the prostate who were to be treated with neoadjuvant hormonal treatment and conformal radiotherapy were

recruited into the study between June 2001 and February 2003. The Local Research Ethics Committee approved the study and written consent was obtained from all men. Histological diagnosis was obtained by transrectal ultrasound guided biopsy in 21 and from tissue obtained at the time of a transurethral resection of the prostate in one. The clinical stage at presentation was T1c – T3b, the modal T-stage being T3 in 14 patients. All men had a negative isotope bone scan. The mean Gleason score was 6 (range, 5 - 8); mean PSA 27.5 ng/ml (range, 6 - 74 ng/ml); and mean age 67 years (range, 57 - 76 years). Following MRI and in accordance with local protocol all men were treated with neoadjuvant hormonal therapy using a luteinizing hormone releasing hormone analogue for 3-4 months and 3D conformal radiotherapy.

Magnetic resonance imaging

MRI was performed at 1.5 T (Gyroscan NT/Intera; Philips Medical Systems, Best, the Netherlands) using a 4-element phased-array receiver coil wrapped around the pelvis. These men were expected to undergo follow-up MRI after radiotherapy thus use of an endorectal receiver was precluded [28]. Following the acquisition of scout images data were acquired encompassing the abdomen and pelvis in both the axial and coronal planes using T_1-weighted spin-echo sequences. These images were used to assess the possibility of extra-prostatic spread. Subsequently, T_2-weighted fast spin echo images of the prostate were obtained in the sagittal and axial planes (field of view = 200 x 200 mm, slice thickness = 3 mm, gap = 0.3 mm, matrix = 256 x 190, repetition time (TR) = 4111 ms, effective echo time (TE) = 135 ms, echo train length 19 and 6 averages). Following the acquisition of quantitative data during contrast agent administration (detailed below), post-contrast T_1-weighted spin echo images of the abdomen and pelvis were again acquired in the axial plane.

Quantitative data encompassing the pelvic region from the apex of the prostate gland into the bladder were acquired using an axial 3D spoiled gradient echo sequence (T_1-FFE with

an elliptical k-space shutter; field of view = 300 x 300 x 100 mm, matrix following interpolation = 128 x 128 x 20, TR = 2.5 ms, TE = 0.86 ms). Prior to contrast agent administration the native T_1 relaxation time was mapped using a series of volume acquisitions with flip angles of 2, 10, 20 and 30 degrees (each acquired with 4 averages). Subsequently, a dynamic series was acquired using a 30-degree flip angle and no averaging over a period of ~4 minutes with a total of 100 to 106 volumes acquired; one every 2.3 s. Contrast agent was administered to the patients through a cannula placed in the antecubital vein prior to scanning. Following the acquisition of the first 5 volumes of the dynamic series 0.1 mmol/kg Gd-DTPA-BMA (Omniscan; Amersham-Health, Little Chalfont, Buckinghamshire, UK) was injected at 3 ml/s using an MRI-compatible power injector (Spectris; Medrad, Indianola, PA). This was immediately followed by a similar volume flush of normal saline.

Data collection and statistical analysis

Data were transferred offline for quantitative analysis. For each patient 4-pixel (22 mm^2) regions of interest were placed (by CR) in the external iliac or femoral arteries (to provide a vascular input function). With the aid of the biopsy results and T_2-weighted images a radiologist (CEH) drew further regions in muscle (internal obturator, selected as a control tissue; region size range 148 to 956 mm^2), hypointense areas within the peripheral zone that were suspected of containing prostate tumor and, where possible, normal contralateral peripheral zone. These regions were drawn to encompass as much tumor and normal contralateral peripheral zone as was visible in the selected slice. Signal intensity variations in these regions were converted to temporal changes in Gd-DTPA-BMA concentration using estimates of native T_1 calculated using the pre-contrast data [29, 30]. Finally, the distributed parameter model described by St. Lawrence and Lee [24] was fitted to the data. Multiple fits were performed to each tissue region using a range of starting points (systematic variation in the initial estimates of τ). The final solution selected was that which minimized the sum of squared differences between the data and the model fit [26, 27]. To determine if differences

existed between vascular characteristics of tumor, normal prostate and muscle in the patients studied parameter estimates were compared using the non-parametric Wilcoxon Signed Ranks test (SPSS for Windows, version 11.5, 2002). Statistical significance was judged at $p < 0.05$.

Results

Magnetic resonance imaging

Data were successfully acquired from all 22 patients. Hypointense lesions were outlined in each patient with reference to the T_2-weighted images and confirmed by reference to the biopsy reports. Normal appearing, hyperintense regions were further outlined in 20 prostates. Example data are presented in Figs. 1 to 3.

Data Analysis

Analysis of the data from the tissue and arterial regions provided estimates of the relaxation and tracer kinetics parameters. Their mean values ± SD are quoted in the text below. The native T_1 relaxation times of tumor, normal-appearing peripheral zone and muscle were 916 ± 298 ms, 962 ± 273 ms and 1026 ± 242 ms, respectively. The model parameter estimates did not follow a normal distribution and the range and median values for each region and parameter are quoted in Table 1. Blood flow in the tumors, 66 ± 43 ml/min/100 ml, was significantly greater than blood flow measured in normal-appearing peripheral zone, 32 ± 36 ml/min/100 ml, ($p < 0.001$) and muscle, 9 ± 7 ml/min/100 ml, ($p < 0.001$). Furthermore, the interstitial volume of contrast agent distribution in tumors, 42 ± 20 ml/100 ml, was larger than that measured in both normal-appearing peripheral zone, 27 ± 10 ml/100 ml, ($p = 0.003$) and muscle, 12 ± 17 ml/100 ml, ($p = 0.002$). The permeability-surface area product of vessels in the tumors, 22 ± 12 ml/min/100 ml, was similar to that measured in normal-appearing tissue, 21 ± 24 ml/min/100 ml, but was higher than seen in muscle, 5 ± 5 ml/min/100 ml, ($p < 0.001$). These trends were lost for estimates of the blood volume where significant differences were not seen. Blood volume estimates in tumors, 1.0 ± 1.4 ml/100 ml, normal-appearing peripheral zone, 1.5 ± 2.4 ml/100 ml, and muscle, 1.8 ± 2.0 ml/100 ml, were all very low. The combined parameter extraction-flow product (K^{trans}/(1-hct)) estimated in tumors, 28 ± 13 ml/min/100 ml, was significantly greater than in normal-appearing peripheral zone, 15 ± 8 ml/min/100 ml, ($p < 0.001$) and muscle, 5 ± 3 ml/min/100 ml, ($p < 0.001$).

Discussion

These findings demonstrate that MRI can be used to estimate parameters only previously measured in the prostate gland using PET [16] or CT [15]. The results confirm that blood flow to tumor tissue exceeds that to normal prostatic tissue but that the difference in blood volume is insignificant [16]. An increase in the interstitial distribution volume, V_e, was measured in tumors [18]. This may explain the high peak enhancement measured in tumors [7] and reflect disruption of the epithelial cell layer surrounding prostatic ducts caused by invading cancer cells [31]. Unlike previous quantitative MRI studies 3D data were acquired encompassing the entire prostate gland. This had the additional advantage of enabling measurement of a vascular input function close to the tissue [30].

Validation. Our estimates of native tissue T_1 made using variable flip angle 3D gradient echo acquisitions [29] compare well with previous measures in both muscle [32] and the prostate [33]. Single capillary distributed parameter models have previously been employed for the analysis of PET data [23] and the St. Lawrence and Lee model specifically has been used in both MRI [26] and CT [15] studies. A variant of the model has been validated in two separate studies for the measurement of blood flow using CT by comparison with microsphere measurements [34, 35]. Though not formally validated in the prostate, simulation studies have indicated that the St. Lawrence and Lee model performs well with comparison to both an independent multiple path distributed parameter model and commonly used compartmental models [27]. In line with previous work [17, 18], the combination of E and F (K^{trans}) measured in the current study was found to be significantly higher in tumor than normal peripheral zone. The estimates of blood flow compare well with estimates made using PET [16]. Even the small decrease in blood volume that was associated with cancer follows the trend observed in that earlier study [16]. Finally, the model-based estimates of blood flow and microvessel PS-product correlate well with the predictions made by pathologists. While tumors contain a greater number of vessels than normal tissue, specifically in angiogenic hot-spots [8], the vessel surface area density in the tumor is

actually reduced [36]. This reflects the size and shape of tumor microvessels that tend to be broad and less branched than those in normal tissue or low grade tumors. This reduced vessel surface area in the high grade cancers is offset by increased blood flow and vessel wall permeability [36], physiological changes that are obscured in the estimate of PS-product and may explain the similarities between the estimates made in tumors and normal tissue.

Study limitations. Though concordant imaging and biopsy results provide a highly specific marker of cancer in the peripheral zone [37] the study lacks a reference standard such as whole-mount prostatectomy specimens [38]. Essential to the analysis of any experiment is data quality. The data acquired from the external iliac/femoral arteries and the prostate gland were of good quality but the signal obtained from the internal obturator muscle suffered from a poor signal-to-noise ratio (SNR) and sporadic motion artifact. Motion interfered with a number of the signal-time courses analyzed and future studies will benefit from image registration prior to data analysis. Conventionally the SNR is addressed at the expense of temporal resolution. This was not an option in this study since it was necessary to acquire data very rapidly so that a distributed parameter model could be used. Indeed, the acquisition time employed is already longer than recommended for similar studies [39]. The limited SNR is a common problem in prostate MRI and may be partly addressed by the application of an endorectal coil [38]. Though certain to improve the signal obtained from the prostate it is unlikely to increase the signal from the artery or muscle. Moreover, the endorectal coil may be contraindicated in the assessment of patients following radiotherapy, such as the subjects studied here [28]. Alternatively, SNR could be improved by the use of a high-field MRI system [40]. These limitations may have influenced the accuracy and precision of the parameter estimates obtained. An earlier study revealed that estimates of blood volume obtained using this implementation of the St. Lawrence and Lee model were low [27] and the current results fall below previous estimates made using PET [16]. This may reflect noise or an inadequate temporal resolution in the experimental data [39] that leads to limitations in definition and integration of the arterial input [20]. It may also indicate the

existence of a limited transendothelial water exchange rate [41, 42]. The influence of such effects may be reduced by further decreasing the sensitivity of the imaging sequence to water exchange (by increasing the flip angle, so-called exchange-minimization [41]). Such an approach further compromises the SNR of the sequence and a practical trade-off must be achieved.

Clinical implications. These results provide new quantitative physiological data concerning the prostate gland. The methods represent an advance on previous MRI studies [7, 18] with measurement of an arterial input function, 3D coverage of the entire prostate gland and absolute estimates of both flow and PS-product. Moreover, similar CT studies lack tissue coverage (only one or two sections may be examined) and the intrinsic tissue contrast of MRI that enables discrimination of tumor and normal peripheral zone tissue [15, 20]. The techniques will allow further studies to characterize tissue types, improve diagnosis and categorize patient prognosis. The promising results obtained using qualitative or heuristic methods could be assessed to identify their underlying physiological basis [7, 22]. Tissue characterization in the current study was limited by the method of region selection dictated by the patient group examined. Nevertheless, concordant imaging and biopsy results providing a highly specific marker of cancer in the peripheral zone [37] guided selection of prostate tumor regions. Future work would benefit from comparison with whole-mount prostatectomy specimens providing an improved reference standard [38].

References

1. El-Gabry EA, Halpern EJ, Strup SE, Gomella LG. Imaging prostate cancer: Current and future applications. Oncology-NY 2001; 15:325-336.
2. Schiebler ML, Tomaszewski JE, Bezzi M, et al. Prostatic-carcinoma and benign prostatic hyperplasia - correlation of high-resolution MR and histopathologic findings. Radiology 1989; 172:131-137.
3. Mirowitz SA, Brown JJ, Heiken JP. Evaluation of the prostate and prostatic carcinoma with gadolinium-enhanced endorectal coil MR imaging. Radiology 1993; 186:153-157.
4. Brown G, Macvicar DA, Ayton V, Husband JE. The role of intravenous contrast enhancement in magnetic resonance imaging of prostatic carcinoma. Clin. Radiol. 1995; 50:601-606.
5. Jager GJ, Ruijter ETG, vanderKaa CA, et al. Dynamic turboFLASH subtraction technique for contrast enhanced MR imaging of the prostate: correlation with histopathologic results. Radiology 1997; 203:645-652.
6. Ogura K, Maekawa S, Okubo K, et al. Dynamic endorectal magnetic resonance imaging for local staging and detection of neurovascular bundle involvement of prostate cancer: Correlation with histopathologic results. Urology 2001; 57:721-726.
7. Engelbrecht MR, Huisman HJ, Laheij RJF, et al. Discrimination of prostate cancer from normal peripheral zone and central gland tissue by using dynamic contrast-enhanced MR imaging. Radiology 2003; 229:248-254.
8. Weidner N, Carroll PR, Flax J, Blumenfeld W, Folkman J. Tumor angiogenesis correlates with metastasis in invasive prostate carcinoma. Am. J. Pathol. 1993; 143:401-409.
9. Brawer MK, Deering RE, Brown M, Preston SD, Bigler SA. Predictors of Pathological Stage in Prostatic Carcinoma - the Role of Neovascularity. Cancer 1994; 73:678-687.
10. Lee TY, Purdie TG, Stewart E. CT imaging of angiogenesis. Q J Nucl Med 2003; 47:171-187.

11. Buckley DL, Drew PJ, Mussurakis S, Monson JRT, Horsman A. Microvessel density in invasive breast cancer assessed by dynamic Gd-DTPA enhanced MRI. J Magn Reson Imaging 1997; 7:461-464.

12. Schlemmer HP, Merkle J, Grobholz R, et al. Can pre-operative contrast-enhanced dynamic MR imaging for prostate cancer predict microvessel density in prostatectomy specimens? Eur. Radiol. 2004; 14:309-317.

13. Tofts PS. Modeling tracer kinetics in dynamic Gd-DTPA MR imaging. J Magn Reson Imaging 1997; 7:91-101.

14. Bassingthwaighte JB, Goresky CA. Modeling in the analysis of solute and water exchange in the microvasculature. In: Renkin EM, Michel CC, Geiger SR, eds. Handbook of physiology - Section 2: The cardiovascular system. Bethesda: American Physiological Society, 1984; 549-626.

15. Henderson E, Milosevic MF, Haider MA, Yeung IWT. Functional CT imaging of prostate cancer. Phys. Med. Biol. 2003; 48:3085-3100.

16. Inaba T. Quantitative measurements of prostatic blood flow and blood volume by positron emission tomography. J Urol 1992; 148:1457-1460.

17. Turnbull LW, Buckley DL, Turnbull LS, Liney GP, Knowles AJ. Differentiation of prostatic carcinoma and benign prostatic hyperplasia: correlation between dynamic Gd-DTPA enhanced MR imaging and histopathology. J Magn Reson Imaging 1999; 9:311-316.

18. Padhani AR, Gapinski CJ, Macvicar DA, et al. Dynamic Contrast Enhanced MRI of Prostate Cancer: Correlation with Morphology and Tumour Stage, Histological Grade and PSA. Clin Radiol 2000; 55:99-109.

19. Muramoto S, Uematsu H, Sadato N, et al. H(2) (15)0 positron emission tomography validation of semiquantitative prostate blood flow determined by double-echo dynamic MRI: a preliminary study. J Comput Assist Tomogr 2002; 26:510-514.

20. Harvey CJ, Blomley MJK, Dawson P, et al. Functional CT imaging of the acute hyperemic response to radiation therapy of the prostate gland: Early experience. J. Comput. Assist. Tomogr. 2001; 25:43-49.

21. Tofts PS, Brix G, Buckley DL, et al. Estimating kinetic parameters from dynamic contrast-enhanced T1-weighted MRI of a diffusable tracer: Standardized quantities and symbols. J Magn Reson Imaging 1999; 10:223-232.

22. Muramoto S, Uematsu H, Kimura H, et al. Differentiation of prostate cancer from benign prostate hypertrophy using dual-echo dynamic contrast MR imaging. Eur. J. Radiol. 2002; 44:52-58.

23. Larson KB, Markham J, Raichle ME. Tracer-kinetic models for measuring cerebral blood flow using externally detected radiotracers. J Cereb Blood Flow Metab 1987; 7:443-463.

24. St Lawrence KS, Lee TY. An adiabatic approximation to the tissue homogeneity model for water exchange in the brain: I. Theoretical derivation. J Cereb Blood Flow Metab 1998; 18:1365-1377.

25. Johnson JA, Wilson TA. A model for capillary exchange. Am. J. Physiol. 1966; 210:1299-1303.

26. Henderson E, Sykes J, Drost D, Weinmann HJ, Rutt BK, Lee TY. Simultaneous MRI measurement of blood flow, blood volume, and capillary permeability in mammary tumors using two different contrast agents. J Magn Reson Imaging 2000; 12:991-1003.

27. Buckley DL. Uncertainty in the analysis of tracer kinetics using dynamic contrast-enhanced T1-weighted MRI. Magn Reson Med 2002; 47:601-606.

28. Maio A, Rifkin MD. Magnetic resonance imaging of prostate cancer - update. Top Magn Reson Imaging 1995; 7:54-68.

29. Brookes JA, Redpath TW, Gilbert FJ, Murray AD, Staff RT. Accuracy of T1 measurement in dynamic contrast-enhanced breast MRI using two- and three-dimensional variable flip angle fast low-angle shot. J Magn Reson Imaging 1999; 9:163-171.

30. Zhu XP, Li KL, Kamaly-Asl ID, et al. Quantification of endothelial permeability, leakage space, and blood volume in brain tumors using combined T1 and T2* contrast-enhanced dynamic MR imaging. J Magn Reson Imaging 2000; 11:575-585.

31. Noworolski SM, Chen AP, Vigneron DB, Kurhanewicz J. Assessment of prostatic ductal volume using combined dynamic contrast-enhanced MRI and diffusion MRI. In:ISMRM 11th Annual Meeting. Toronto, Ontario, 2003; 1464.

32. de Certaines JD, Henriksen O, Spisni A, Cortsen M, Ring PB. In vivo measurements of proton relaxation times in human brain, liver, and skeletal muscle: a multicenter MRI study. Magn Reson Imaging 1993; 11:841-850.

33. Kjaer L, Thomsen C, Iversen P, Henriksen O. In vivo estimation of relaxation processes in benign hyperplasia and carcinoma of the prostate gland by magnetic resonance imaging. Magn Reson Imaging 1987; 5:23-30.

34. Cenic A, Nabavi DG, Craen RA, Gelb AW, Lee TY. A CT method to measure hemodynamics in brain tumors: Validation and application of cerebral blood flow maps. Am J Neuroradiol 2000; 21:462-470.

35. Purdie TG, Henderson E, Lee TY. Functional CT imaging of angiogenesis in rabbit VX2 soft-tissue tumour. Phys. Med. Biol. 2001; 46:3161-3175.

36. Barth PJ, Weingartner K, Kohler HH, Bittinger A. Assessment of the vascularization in prostatic carcinoma: A morphometric investigation. Hum. Pathol. 1996; 27:1306-1310.

37. Wefer AE, Hricak H, Vigneron DB, et al. Sextant Localization of Prostate Cancer: Comparison of Sextant Biopsy, Magnetic Resonance Imaging and Magnetic Resonance Spectroscopic Imaging With Step Section Histology. J Urol 2000; 164:400-404.

38. Quinn SF, Franzini DA, Demlow TA, Rosencrantz DR, Kim J, Hanna RM. MR imaging of prostate cancer with an endorectal surface coil technique: correlation with whole-mount specimens. Radiology 1994; 190:323-327.

39. Henderson E, Rutt BK, Lee TY. Temporal sampling requirements for the tracer kinetics modeling of breast disease. Magn Reson Imaging 1998; 16:1057-1073.

40. Kim HW, Buckley DL, Peterson DM, et al. In vivo prostate magnetic resonance imaging and magnetic resonance spectroscopy at 3 Tesla using a transceive pelvic phased array coil - Preliminary results. Invest. Radiol. 2003; 38:443-451.

41. Donahue KM, Weisskoff RM, Chesler DA, et al. Improving MR quantification of regional blood volume with intravascular T1 contrast agents: accuracy, precision, and water exchange. Magn Reson Med 1996; 36:858-867.

42. Buckley DL. The influence of transcapillary water exchange on the analysis of tracer kinetics in dynamic Gd-DTPA-enhanced T1-weighted MRI. In:ISMRM 10th Annual Meeting. Honolulu, Hawaii, 2002; 2120.

Table 1: Median value (and interquartile range) of the estimates of flow (F), blood volume (V_b), microvascular permeability-surface area product (PS) and interstitial volume (V_e) in prostate tumors, normal-appearing peripheral zone and nearby muscle.

region	F *(ml/100 ml/min)*	V_b *(ml/100 ml)*	PS* *(ml/100 ml/min)*	V_e *(ml/100 ml)*
tumor (n = 22)	57 (30 – 81)	0.4 (0.2 – 1.2)	19 (13 – 32)	38 (27 – 50)
normal (n = 20)	18 (13 – 32)	0.4 (0.0 – 2.1)	16 (7 – 26)	25 (19 – 34)
muscle (n = 22)	7 (5 – 12)	1.2 (0.4 – 2.6)	5 (2 – 6)	6 (4 – 12)

*Unable to determine PS when E = 1. Results quoted for n = 22; n = 17; n = 20.

Figure captions

Fig. 1 Tissue enhancement following bolus administration of Gd-DTPA-BMA. Axial T_2-weighted turbo spin echo image (TR/TE 4111/135 ms) of an example patient showing the prostate gland (a). Regions of interest have been drawn to outline tumor (left/anterior of the prostate) and contralateral normal-appearing peripheral zone (right side of the prostate). The graphs illustrate enhancement over time in the external iliac artery (faint lines, scaled down by a factor of 10), tumor (b) and normal (c) regions. In each graph the bold line represents the best fit of the model to the data and provides estimates of (amongst other parameters) blood flow, F, and interstitial distribution volume, V_e. (b) Tumor tissue. F = 109 ml/100 ml/min and V_e = 30 ml/100 ml. (c) Normal tissue. F = 21 ml/100 ml/min and V_e = 34 ml/100 ml.

Fig. 2 (a) Axial T_2-weighted turbo spin echo image (TR/TE 4111/135 ms) of a second example patient showing the prostate gland with tumor in the left posterior area of the gland. (b) Graph illustrates enhancement over time in tumor (open squares), normal (filled circles) and muscle (open circles) regions. The bold lines represent the best fit of the model to the data. Parameter estimates were obtained for tumor, F = 64 ml/100 ml/min and V_e = 50 ml/100 ml; normal, F = 19 ml/100 ml/min and V_e = 40 ml/100 ml; muscle, F = 12 ml/100 ml/min and V_e = 7 ml/100 ml.

Fig. 3 (a) Axial T_2-weighted turbo spin echo image (TR/TE 4111/135 ms) of a third example patient showing the prostate gland with tumor in the left posterior area of the gland. (b) Graph illustrates enhancement over time in tumor (open squares), normal (filled circles) and muscle (open circles) regions. The bold lines represent the best fit of the model to the data. Note the noise in the muscle data and the undulating nature of the model fits reflecting variability in this patient's arterial input function. Parameter estimates were obtained for tumor, F = 132 ml/100 ml/min and V_e = 55 ml/100 ml; normal, F = 109 ml/100 ml/min and V_e = 40 ml/100 ml; muscle, F = 8 ml/100 ml/min and V_e = 18 ml/100 ml.

Figure 1

a.

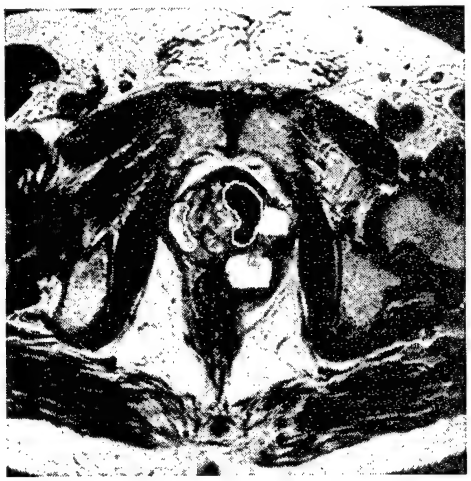

b.

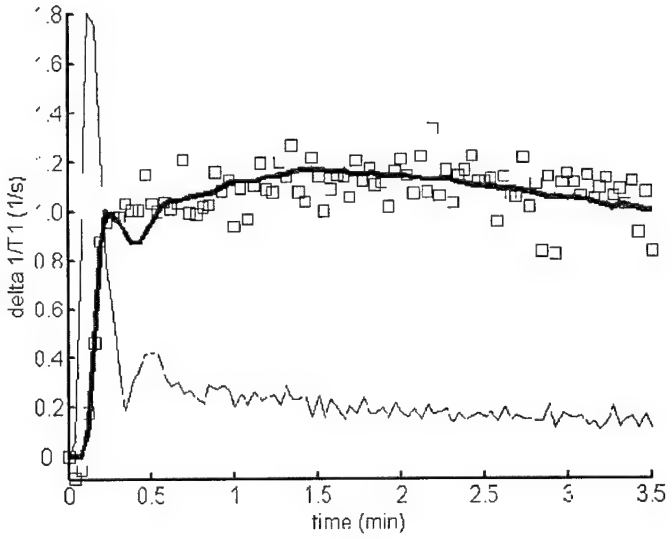

c.

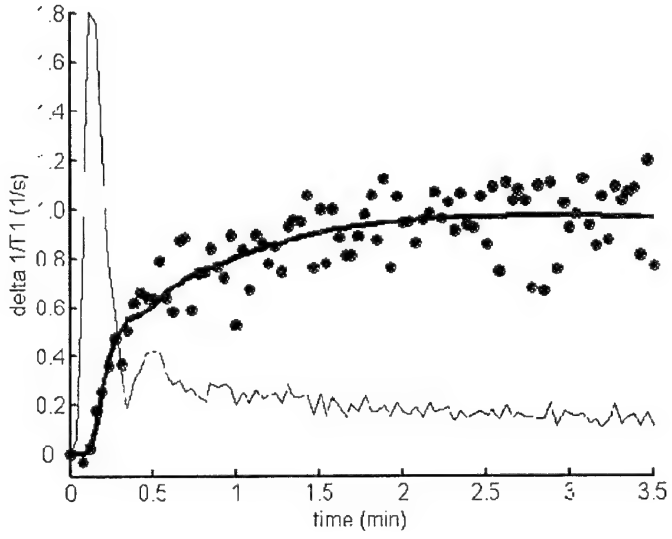

Figure 2

a.

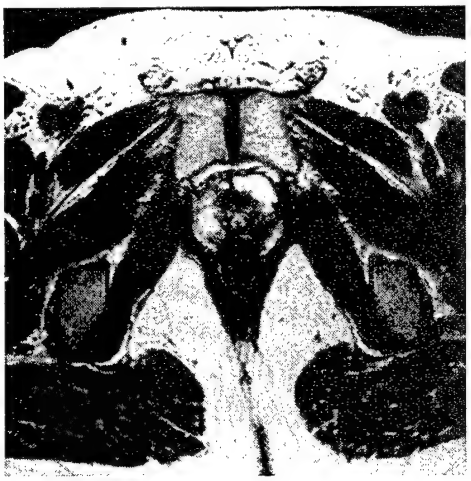

b.

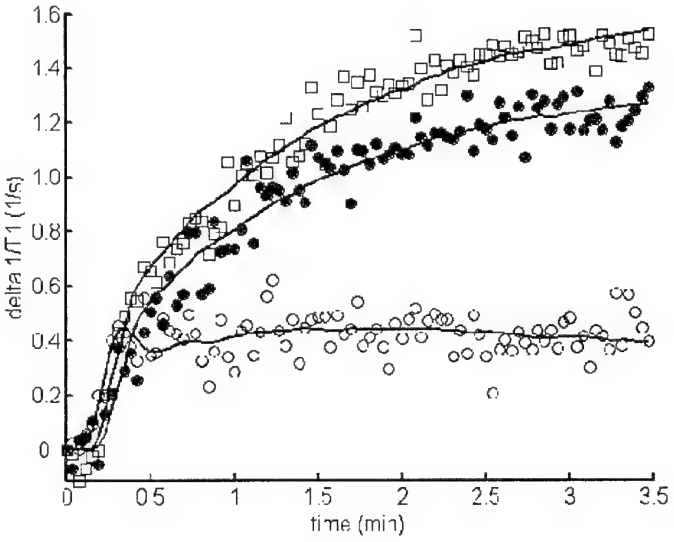

Figure 3

a.

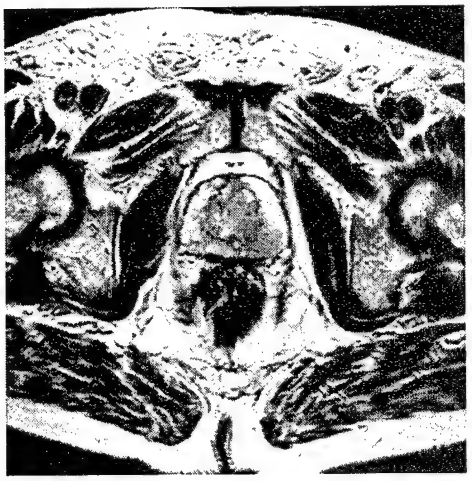

b.

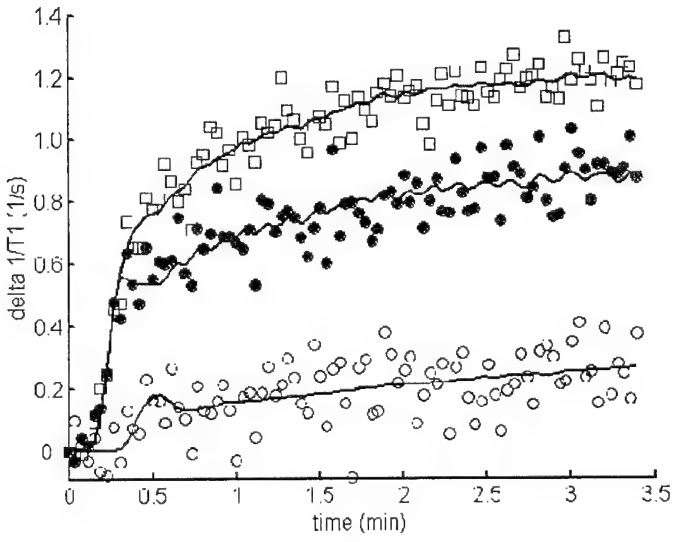

Characterization of prostate cancer by quantitative MRI

D. L. Buckley[1], C. Roberts[1], S. K. Khaki[1], G. J. Parker[1], J. P. Logue[2], C. E. Hutchinson[1]

[1]Imaging Science and Biomedical Engineering, University of Manchester, Manchester, United Kingdom, [2]Department of Clinical Oncology, Christie Hospital, Manchester, United Kingdom

Introduction.

Quantitative estimates of the baseline physiology and MR characteristics of the prostate may help to predict the response of the gland to treatment. The purpose of this study was to assess these characteristics in the pathological prostate gland prior to treatment with external beam radiotherapy using T_1 and T_2 mapping, dynamic contrast-enhanced MRI and a distributed parameter tracer kinetic model. The hypothesis to be tested is that these characteristics will serve as sensitive indicators of tissue response to treatment and thereby provide a useful prognostic tool.

Methods.

Twenty-two men with histologically proven adenocarcinoma of the prostate were recruited into the study. The Local Research Ethics Committee approved the study and written consent was obtained from all men. Histological diagnosis was obtained by transrectal ultrasound guided biopsy in 21 and from tissue obtained at the time of a transurethral resection of the prostate in one. The clinical stage at presentation was T1c – T3b. All men had a negative isotope bone scan. The mean Gleason score was 6 (range, 5 - 8); mean PSA 27.5 ng/ml (range, 6 - 74 ng/ml) and mean age 67 years (range, 57 - 76 years). These patients all selected external beam radiotherapy for subsequent treatment of their disease. The patients were scanned on a 1.5 T Philips MR system using a pelvic phased-array coil. T_2-weighted fast spin echo images of the entire gland were acquired using a TR of 4.75 s at echo times of 7, 45, 100 and 240 ms to estimate baseline T_2 [1]. A 3D T_1-weighted gradient echo pulse sequence was used at flip angles of 2°, 10°, 20° and 30° to estimate baseline T_1 [2]. This was followed by a dynamic series in which volumes (flip angle 30°) were acquired every 2.3 s for approximately 4 minutes. Early in this series 0.1 mmol/kg Gd-DTPA-BMA was injected at 3 ml/s using a power injector.

The image data were subsequently analysed off-line. For each patient regions of interest were drawn in the external iliac or femoral arteries (to provide a vascular input function). With the aid of T_2-weighted images a radiologist (CEH) drew further regions in prostate tumour, muscle (internal obturator) and, where possible, normal contralateral peripheral zone. For each region estimates of T_1 and T_2 were made and signal intensity variations were converted to temporal changes in Gd-DTPA-BMA concentration [2] and a distributed parameter model [3] was fitted to the data.

Results.

Analysis of the data from each region provided estimates (mean ± SD) of T_1, T_2, blood flow (F), blood volume (V_b), microvascular permeability-surface area product (PS) and interstitial volume (V_e) [4].

Tissue	T_1 (ms)	T_2 (ms)	F (ml/100 ml/min)	V_b (ml/100 ml)	PS (ml/100 ml/min)	V_e (ml/100 ml)
Tumour (n=22)	916 ± 298	93 ± 15	66 ± 43	1.0 ± 1.4	22 ± 12	42 ± 20
Normal (n=20)	962 ± 273	131 ± 27*	32 ± 36*	1.5 ± 2.4	21 ± 24	27 ± 10*
Muscle (n=22)	1026 ± 242	52 ± 8*	9 ± 7*	1.8 ± 2.0	5 ± 5*	12 ± 17*

*Significantly different from tumour values using the non-parametric Wilcoxon Signed Ranks test ($p<0.01$).

Discussion.

Our estimates of the relaxation times compare well with previous results and underscore the drop in T_2 seen in cancer [1]. This analysis was based upon estimates of T_2 made using only the first three echoes. There was an indication of the multiexponential T_2 behaviour reported by Kjaer et al. [5] when the 240 ms echo data were considered and this finding requires further study.

The results of the tracer kinetics analysis confirm that blood flow to tumour tissue exceeds that to normal prostatic tissue but that the difference in blood volume is insignificant [6]. Similarly, the interstitial distribution space in the tumours is enlarged [7] but no difference between the permeability-surface area products of tumour and normal microvessels was detectable. In a recent publication reporting the use of contrast-enhanced CT and the same tracer kinetics model the authors stressed the importance of interpreting results with caution since the precision of parameter estimates can be low [8]. Indeed, the estimates of PS made in this study were not always reliable; PS cannot be estimated when the contrast agent is completely extracted on its first pass (E = 1). The blood volume estimates reported by Henderson et al. [8] were larger than found in this study and may reflect MR-specific problems associated with transendothelial water exchange [9] in addition to the difficulties previously experienced in fitting complex models [4]. However, MR studies such as this have distinct advantages over CT studies. The exquisite soft tissue contrast of T_2-weighted images allows for the analysis of hypointense regions against normal-appearing peripheral zone in any part of the gland. The radiation burden of the dynamic CT study prevents the examination of more than one or two sections and these must be chosen with little prior knowledge of the location of cancer. MR may be used repeatedly; further studies are ongoing with patients returning for follow-up MR scans 12 months after treatment. These findings show considerable promise for isolating both the MR and physiological characteristics of prostate cancer and may help to assess tissue response to treatment in this and future studies.

Acknowledgments. Funded by the U.S. Department of Defense Prostate Cancer Research Program (PC991154). Jeanette Lyons, Yvonne Watson and David Clark kindly helped with the patient studies.

References. **1.** Liney GP et al. *Magn Reson Imaging* 15:1177-1186 (1997); **2.** Zhu XP et al. *J Magn Reson Imaging* 11:575-585 (2000); **3.** St. Lawrence KS, Lee TY *J Cereb Blood Flow Metab* 18:1365-1377 (1998); **4.** Buckley DL *Magn Reson Med* 47:601-606 (2002); **5.** Kjaer L et al. *Magn Reson Imaging* 5:23-30 (1987); **6.** Inaba T *J Urol* 148:1457-1460 (1992); **7.** Padhani AR et al. *Clin Radiol* 55:99-109 (2000); **8.** Henderson E et al. *Phys Med Biol* 48:3085-3100 (2003); **9.** Buckley DL *Proc. 10th meeting ISMRM*, Honolulu, 2120 (2002).

NOTES

Magnetic Resonance in Medicine 47:601–606 (2002)
DOI 10.1002/mrm.10080

Uncertainty in the Analysis of Tracer Kinetics Using Dynamic Contrast-Enhanced T_1-Weighted MRI

David L. Buckley*

In recent years a number of physiological models have gained prominence in the analysis of dynamic contrast-enhanced T_1-weighted MRI data. However, there remains little evidence to support their use in estimating the absolute values of tissue physiological parameters such as perfusion, capillary permeability, and blood volume. In an attempt to address this issue, data were simulated using a distributed pathway model of tracer kinetics, and three published models were fitted to the resultant concentration-time curves. Parameter estimates obtained from these fits were compared with the parameters used for the simulations. The results indicate that the use of commonly accepted models leads to systematic overestimation of the transfer constant, K^{trans}, and potentially large underestimates of the blood plasma volume fraction, V_p. In summary, proposals for a practical approach to physiological modeling using MRI data are outlined. Magn Reson Med 47:601–606, 2002.

Key words: perfusion; gadolinium; carcinoma; kinetic modeling; capillary permeability; blood volume

The last decade has seen a rapid development in the use of dynamic contrast-enhanced T_1-weighted MRI in medicine. In tandem with the technological advances that have enabled improved data acquisition, a number of investigators have employed physiological models to facilitate data interpretation. While the use of these models has found numerous applications (e.g., in studies of tumor physiology (1) and myocardial perfusion (2)), and a number of groups have assessed the potential of model parameters as surrogate markers (3,4), little has been published that addresses the direct interpretation of these results. Specifically, how do the estimates obtained using the various models compare with the physiological parameters they purport to measure?

This is not a simple question to address since it is often difficult to identify a reliable "gold standard." Many investigators compare their results with those obtained with positron emission tomography (PET). However, PET shares many of the basic models employed in MRI (5). Similarly, data simulation exercises using Monte-Carlo techniques designed to assess accuracy and precision in parameter estimation often utilize the same model to both generate and analyze the data (6,7). In this way, the sensitivity of the estimates to experimental variables, such as noise and sampling frequency, is assessed but little is revealed about the physiological significance of the resultant parameter estimates.

A physiological model incorporating multiple parallel pathways and heterogeneous flow was used to simulate data of a realistic nature to which simplified models were fitted. The experiment was designed to assess the accuracy of the models themselves, not the quality of the data to which they are fitted (in terms of noise, sampling frequency, etc.), since data quality is essentially an experimental variable. Furthermore, this study was restricted to those models dealing with a contrast agent that diffuses out of the vascular space (thereby incorporating capillary permeability as a model parameter). Many of the issues associated with the analysis of data from susceptibility contrast studies, which typically assume that the contrast agent remains intravascular, have been investigated in previous studies (e.g., Refs. 7 and 8). Data were simulated using the distributed pathway model of tracer kinetics called the multiple indicator, multiple path, indicator dilution 4 region model (MMID4), made available by the National Simulation Resource (Department of Bioengineering, University of Washington). These data were subsequently analyzed using three different tracer kinetic models, and the parameter estimates obtained were compared with the physiological variables used in the MMID4 model.

Out of necessity, only a few models and the underlying assumptions that support these models can be examined. The use of a fixed input function (originally proposed by Tofts and Kermode (9)) is known to introduce considerable error into the estimate of the capillary permeability-surface area product (10). Given this, the following analyses assume that the arterial input function has been measured. Although techniques to achieve this are not yet in common use, an increasing number of investigators are developing practical methods for doing so (11,12).

METHODS

Data Simulation

Tissue residue curves were simulated using the MMID4. This model (described in detail in Refs. 13 and 14) accounts for flow dispersion and heterogeneity, and includes capillaries modeled as axially distributed blood–tissue exchange units. A plasma concentration-time curve was simulated as an input to the model. The amplitude and shape of the curve were based upon measurements made in the

Imaging Science and Biomedical Engineering, University of Manchester, Manchester, UK.

Grant sponsor: U.S. Department of Defense Prostate Cancer Research Program; Grant number: PC991154; Grant sponsor: NIH; Grant number: RO1 NS36992.

*Correspondence to: David L. Buckley, Ph.D., Imaging Science and Biomedical Engineering, University of Manchester, Stopford Building, Oxford Road, Manchester M13 9PT, UK. E-mail: david.buckley@man.ac.uk

Received 6 September 2001; revised 22 October 2001; accepted 22 October 2001.

descending aorta of volunteers following bolus injection of Gd-DTPA (11). Reference data for comparison with the simulated residue curves were obtained from MR studies of human brain, breast, and prostate tumors (15).

Numerous parameters determine the behavior of the MMID4 model. Delay and dispersion of the arterial input were set to zero. Contrast agent in nonexchanging vessels (arteries, arterioles, venules, and veins) may contribute to the tissue residue function. However, such vessels were excluded in this study, as the tumors of interest are likely to contain a predominance of newly formed, leaky vessels (16). Flow heterogeneity was modeled by apportioning flow through 20 parallel pathways according to a right-skewed lagged normal density distribution (14). For the sake of clarity a tissue density of 1 g/ml was assumed for all model analyses (17). Other than mean plasma flow (F_p) the only parameters that were adjusted in the simulations were those associated with blood–tissue exchange: capillary plasma volume (V_p), capillary permeability-surface area product (PS), and interstitial volume (V_e).

Model Fitting

Three models were chosen for assessment. Model 1, the modified Kety model (18), was essentially applied to MRI data by both Larsson et al. (19) and Tofts and Kermode (9):

$$C_{tis}(t) = EF_p \int_0^t C_p(u)\exp\left(\frac{-EF_p}{V_e}(t-u)\right)du \qquad [1]$$

where C_{tis} and C_p are the concentrations of contrast agent in the tissue of interest and plasma, respectively, and the extraction fraction, $E = 1 - \exp(-PS/F_p)$. In accord with recent standardization, it is important to stress that the product EF_p may also be referred to as K^{trans} (20). Model 2 resembles the first, but includes a vascular term (17) and has been used to analyze MR data in a number of studies (2,6):

$$C_{tis}(t) = V_pC_p(t) + EF_p \int_0^t C_p(u)\exp\left(\frac{-EF_p}{V_e}(t-u)\right)du. \qquad [2]$$

Model 3, recently described by St. Lawrence and Lee (21), potentially enables the estimation of F_p and PS separately:

$$C_{tis}(t) = F_p \int_0^\tau C_p(t-u)du + EF_p \int_\tau^t C_p(u) \times \exp\left(\frac{-EF_p}{V_e}(t-u-\tau)\right)du \qquad [3]$$

where τ is the mean capillary transit time ($= V_p/F_p$). Model 1 has two unknown parameters that may be estimated by curve fitting: the product EF_p and the interstitial volume V_e. Model 2 has three unknown parameters: the product EF_p, the interstitial volume V_e, and the plasma volume V_p. Model 3 contains four unknown parameters that may be estimated by curve fitting: F_p, E, V_e, and τ. From these, the parameters PS and V_p may be evaluated.

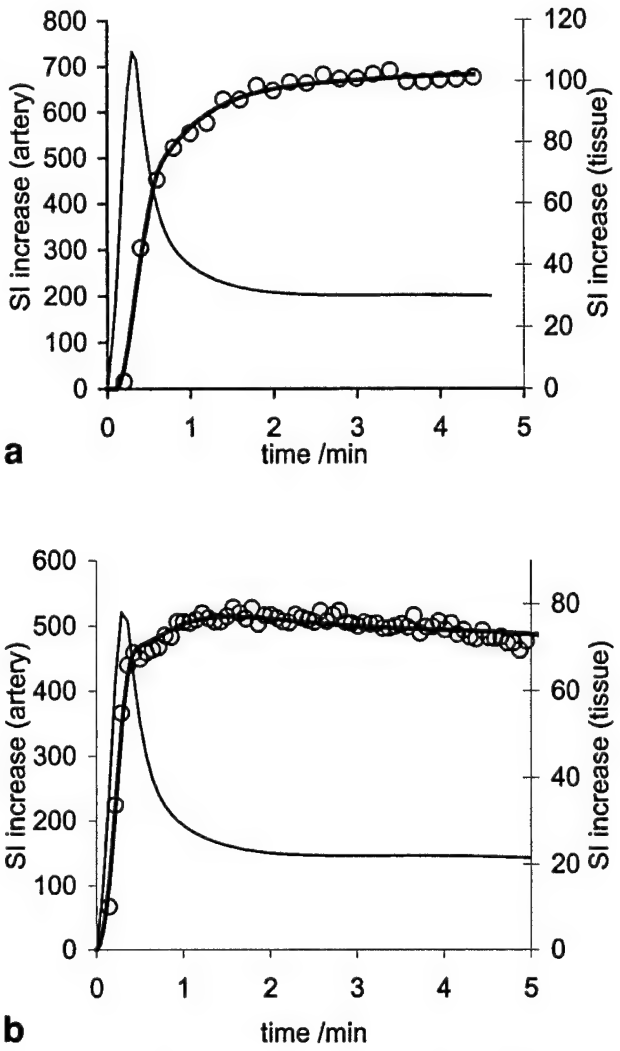

FIG. 1. Representative signal-time curves used for simulations. Tissue signal-time curves (bold lines) simulated using an assumed arterial input function (faint lines), MMID4, and the physiological parameters: (a) F_p, 0.57 ml/g/min; V_p, 0.06 ml/g; PS, 0.33 ml/g/min; V_e, 0.45 ml/g; and (b) F_p, 1.2 ml/g/min; V_p, 0.08 ml/g; PS, 0.34 ml/g/min; V_e, 0.40 ml/g. Reference data (open circles) were obtained from studies of (a) a breast tumor and (b) a meningioma.

Simulated data were generated in two series. The first series was designed to be representative of data acquired from a breast tumor, and the second was representative of data acquired from a meningioma (Fig. 1). Baseline values selected for V_p and V_e were based on estimates from the literature. These values were then held fixed while MMID4, with only F_p and PS as free parameters, was fitted to the reference data. Best-fit estimates of F_p and PS combined with the choices of V_p and V_e were then used as baseline values for the simulated data. In each case points were calculated with a sampling frequency of one acquisition per second over a total sampling period of 5 min. Twenty-six tissue residue curves were produced using the range of parameter values outlined in Table 1 (Fig. 2). In each case one parameter value (F_p, V_p, or PS) was modified from the baseline values per curve. Four values of each

Table 1
Values of the Adjustable Kinetic Parameters Describing the Behavior of MMID4 Used to Simulate 26 Different Tissue Residue Curves

	Baseline	Exps. 2–5	Exps. 6–9	Exps. 10–13
(a) Data representative of a breast tumor				
F_p (ml/min/g)	0.57	0.17, 0.37, 0.77, 0.97	0.57	0.57
V_p (ml/g)	0.06	0.06	0.0001, 0.03, 0.09, 0.12	0.06
PS (ml/min/g)	0.33	0.33	0.33	0.01, 0.17, 0.49, 0.65
V_e (ml/g)	0.45	0.45	0.45	0.45
(b) Data representative of a meningioma				
F_p (ml/min/g)	1.2	0.4, 0.8, 1.6, 2.0	1.2	1.2
V_p (ml/g)	0.08	0.08	0.0001, 0.04, 0.12, 0.16	0.08
PS (ml/min/g)	0.34	0.34	0.34	0.0, 0.17, 0.51, 0.68
V_e (ml/g)	0.4	0.4	0.4	0.4

The remaining parameters associated with MMID4 were held fixed (see text). A representative selection of the resultant tissue residue curves is shown in Fig. 2.

parameter were chosen in addition to the baseline values; thus, 13 curves were generated per series. Each of the three models in turn was fitted to the 26 simulated data sets and estimates of the parameters were compared with the values used in MMID4 to generate the residue curves.

RESULTS

Data Simulation

The simulated data exhibit many of the characteristics of the experimental data (Fig. 1). Indeed the simulated data match the example data very well despite the arterial input function used (a single simulated input not determined in individual subjects). The physiological parameters influence the residue curves in different ways (Fig. 2). The initial slope of the residue curve is determined principally by the vascular parameters. The early curvature and peak observed in the data is strongly influenced by PS. There is, however, considerable overlap of these effects.

Model Fitting

Models 1 and 2 fitted the simulated data in a reproducible manner. Parameter estimates obtained from these fits are displayed in Fig. 3. Parameter estimates obtained using model 3 were not always unique, and often depended on the starting guesses used in the fitting routine. This implies a significant correlation between parameters and the existence of local minima (22). To improve the stability of the regression procedure, an approach similar to that de-

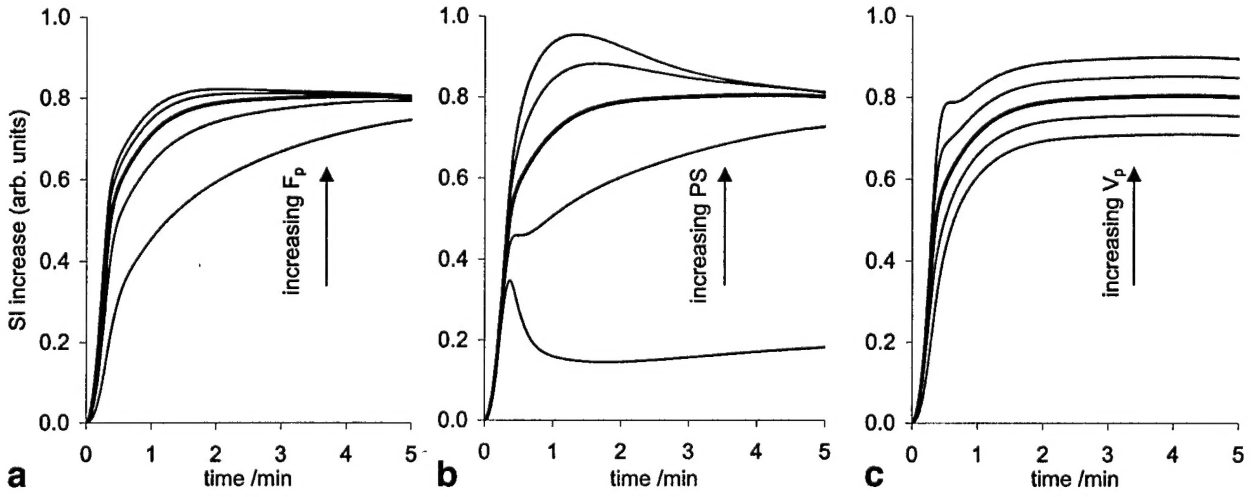

FIG. 2. Influence of the physiological parameters. The shape of the signal-time curve is modified by changes in the values of individual parameters. The baseline curve (bold line) is representative of data acquired from a breast tumor. The influence of changes in (**a**) plasma flow (F_p), (**b**) permeability-surface area product (PS), and (**c**) plasma volume (V_p) are shown. The parameter values used to generate the curves are detailed in Table 1a.

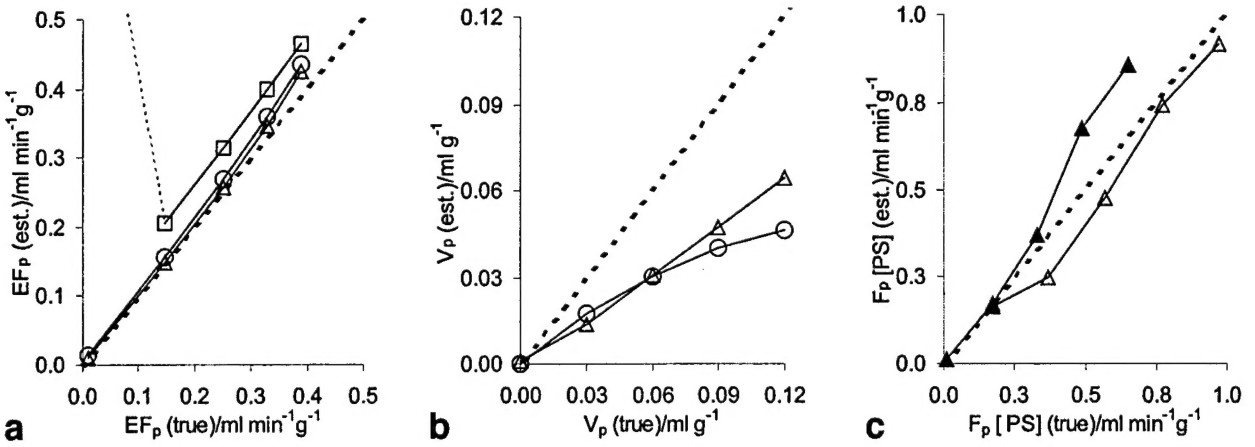

FIG. 3. Parameter estimates as a function of the "true" values. Estimates of the parameters (**a**) EF_p, (**b**) V_p, and (**c**) F_p and PS obtained by fitting model 1 (squares), model 2 (circles), and model 3 (triangles) to the simulated data (Table 1a). The open triangles in **c** represent estimates of F_p, the filled triangles represent estimates of PS, and the dashed lines in all figures represent lines of identity. Similar plots were obtained using the parameters of Table 1b. **a:** Note the failure of model 1 at low EF_p (0.01 ml $min^{-1}g^{-1}$). The model 1 estimate is off-scale at 0.82 ml $min^{-1}g^{-1}$.

scribed by Henderson et al. (22) was adopted. Multiple fits were performed using a range of starting points (i.e., different initial estimates of τ). The final solution selected was that which minimized the sum of squared differences between the data and the model fit. Representative results are displayed in Fig. 3. Though the results in general were convoluted, certain trends were apparent. In particular, V_p was consistently underestimated by both model 2 and model 3 (by between 2% and 96%). The parameters of model 3 became less accurate at low flow or high permeability, where PS tended to be overestimated (to an extreme of 152%) and F_p was slightly underestimated (up to 34%).

DISCUSSION

Increasing numbers of investigators are employing models to analyze their dynamic contrast-enhanced data (20). It is important that the techniques used are fully understood so that they may benefit other investigators. Part of this process is to investigate the physiological interpretation of these parameters. Typically, this would be achieved by comparison of the MRI results with a "gold standard." However, suitable techniques for comparison are difficult to find. PET has often been quoted as a gold standard technique for measurement of blood flow (8), but the techniques used to interpret PET data are very similar to those now used in MRI and can suffer from similar pitfalls (5). In this study, a realistic, established model has been used to simulate tissue residue curves that closely match existing experimental data. In this way, data were generated with known physiological variables that were independent of the models subsequently used to interpret them.

Data Simulation

MMID4 is clearly capable of generating residue curves that closely match experimental data acquired by MRI (8,14,23) (Fig. 1). This should not be interpreted as suggesting that MMID4 fully describes the physiology of the tumors studied. It is simply a step towards that goal. However, MMID4 does incorporate parameters of particular interest: F_p, PS, V_e, and V_p, and each influences the residue curve over differing temporal ranges and in subtly different ways (Fig. 2). F_p, for example, determines the initial slope of the residue curves simulated in this study. PS has a more convoluted impact depending upon the ratio PS:F_p. Certainly, the curvature of the residue curve about the initial peak (Fig. 2) is strongly influenced by PS. V_e has perhaps the clearest affect upon the residue curve. Increasing V_e tends to delay the rise of the curve to its equilibrium amplitude. Finally, the impact of V_p is seen throughout the time course. It is the overlap in influence of each variable that complicates the issue of parameter estimation.

Model Fitting

A model, by definition, is a practical simplification of the true tissue physiology; as a result it is, to some extent, flawed. It is therefore not surprising that the simple models tested were unable to provide accurate estimates of the physiological parameters in all cases. Model 3 bears the closest resemblance to MMID4 but clearly fails to describe the more complex model in certain circumstances. In particular, model 3 systematically underestimates V_p and overestimates PS under conditions of low flow or high permeability (Fig. 3). This may be a consequence of flow heterogeneity (14), an effect all three models overlook. Flow heterogeneity differs between regions and individuals and may not remain constant, as assumed in this study, but could change as a function of pathology (8). The effect of additional disrupting influences on the input function—delay and dispersion—have, for the sake of conciseness, not been considered in this study since their influence upon parameter estimation has been studied elsewhere (7).

If the direct vascular contribution to the signal is ignored (model 1), EF_p (also known as K^{trans} (20)) is overestimated (by up to 54% (Fig. 3a)). Indeed, under certain circum-

stances model 1 breaks down completely. However, to measure the vascular signal contribution it is essential to measure the vascular input and acquire data with a high temporal resolution (6). The choice of model 3 for data analysis requires a sampling interval less than the mean transit time of the tracer. Once the sampling interval reaches the mean transit time, model 3 may be simplified to a form similar to model 2 (21). It is clear from Fig. 3 that the use of model 2, despite the inclusion of a vascular contribution, leads to consistent underestimation of V_p and a slight overestimation of EF_p. These findings mirror the results of a previous study (21). Interestingly, the ratio EF_p:V_e may be estimated with an error of less than 10%, which is consistently less than the error in the estimate of EF_p alone (data not shown). This ratio, otherwise referred to as k_{ep} (20), may be estimated without a tissue T_1 measurement (19), and has been identified as a useful parameter for differential diagnosis in the study of primary breast tumors (24).

Another important issue, which is not always apparent to the investigator, is the uniqueness of the model solution (23). Many of the estimates obtained, using model 3, varied as a function of the starting values used for curve fitting. The array of local minima result from parameter correlations, i.e., different combinations of the parameters produce very similar solutions. Parameter correlations may be examined using sensitivity functions (13) or by examination of the fit correlation matrix. Parameter estimation is simplified if the complexity of the fit can be reduced. It is possible to use MMID4 for data analysis (14,23), but the issue of parameter uniqueness is further complicated by the surfeit of possible parameter combinations. Jerosch-Herold et al. (23), studying myocardial blood flow and capillary permeability in a porcine model, found that they were unable to obtain unique estimates of blood flow, volume, and PS using an extracellular contrast agent (Gd-DTPA). They were able to assess blood flow using an experimental intravascular tracer, as all the extravascular parameters were eliminated as degrees of freedom of the model. Even under these circumstances, it was necessary to fix the value of numerous additional MMID4 parameters at literature values (23). It is likely that future studies may benefit from the combined use of intravascular and extracellular tracers in multiple-indicator-type modeling (13). Indeed, model 3 has been tested with two different contrast agents (22) in a canine model of breast cancer. Furthermore, Henderson et al. (22) recognized the confounding impact of parameter correlations upon parameter estimation. To overcome this problem, curve fitting was performed in a serial fashion using a succession of starting points for the fit (22), a policy adopted in this study.

Implications for Tracer Kinetic Studies

It is important at the outset of a study to identify the most relevant parameters to measure. Without an arterial input function and with limited temporal resolution, the Tofts and Kermode (9) and Larsson et al. (19) models have proved very useful. In tissues with a negligible blood volume they may also provide good estimates of EF_p. However, with a measured arterial input function and rapid data collection, model 2 may be a more appropriate model

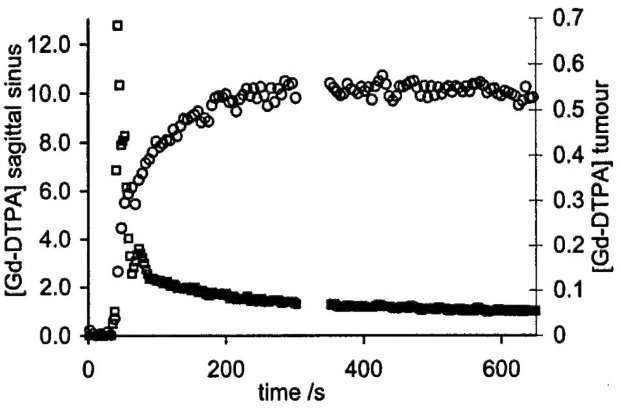

FIG. 4. Measurement of the arterial and tissue concentrations in vivo. Given an appropriate imaging sequence the arterial input function and the tissue residue curve can be measured in vivo. These data were acquired from regions of interest encompassing the sagittal sinus (open squares) and a meningioma (open circles). Calculation of the concentration of Gd-DTPA (mM) was based upon precontrast T_1 measurement (12).

for clinical data evaluation. In either case the investigator must appreciate the assumptions and implications of using these models. In particular, neither model provides separate estimates of perfusion and permeability. These parameters are inextricably combined in the EF_p product. The model (model 3) of St. Lawrence and Lee (21) offers the possibility of assessing blood flow and extraction simultaneously, but may require carefully constrained supervised data fitting (22), additional measurements, or multiple tracers to overcome problems with parameter correlations (23). In all cases it is essential to collect appropriate data of the highest quality if accuracy and precision are to be attained.

As a practical example of these choices, the models were each fitted to recent experimental data (input and tissue residue curves) acquired in a meningioma (12), shown in Fig. 4. These data were simultaneously acquired every 5.1 s in the sagittal sinus and tumor using a T_1-weighted 3D gradient-echo sequence (TR = 4.3 ms, TE = 1.1 ms, flip angle = 35°) on a 1.5 T MR system. The signal from the sagittal sinus was used as input to the models (a vein was chosen for simplicity and is merely illustrative) and the effective sampling interval was halved by linear interpolation. The following parameter estimates were obtained using model 3: blood (rather than plasma) flow, F_b = 0.25 ml $min^{-1}g^{-1}$; blood volume, V_b = 0.02 ml g^{-1}; V_e = 0.43 ml g^{-1}; and PS = 0.14 ml $min^{-1}g^{-1}$. It is unclear whether the interpolation step was required since the capillary transit time, τ, was estimated to be 4.8 s. Based on the results of the previous simulation exercise, PS and F_b may be somewhat overestimated and underestimated, respectively. Furthermore, the estimate of V_b is likely to represent a significant underestimate. However, the product EF_b (= 0.16 ml $min^{-1}g^{-1}$) is likely to be accurately estimated, and these results compare well with estimates obtained using model 2: EF_b = 0.16 ml $min^{-1}g^{-1}$; V_b = 0.02 ml g^{-1}; and V_e = 0.44 ml g^{-1}. Predictably, the estimate of the EF_b product made by model 1 was larger (0.18 ml

$min^{-1}g^{-1}$) but a comparable value was obtained for V_e (0.44 ml g^{-1}). Unless an independent estimate of blood flow or permeability is essential, model 2 may be an appropriate choice for analysis of these data since it requires neither data interpolation nor supervised fitting.

CONCLUSIONS

The use of models for tracer kinetic analysis potentially enables the investigator to interpret MR data in physiological terms. However, both the measurement process and the data analysis introduce a degree of uncertainty into parameter estimation. Simplified models, some of which are in common use, may not provide accurate estimates of the physiological parameters of interest. It is important to address these uncertainties because it is only after the parameters of the model have been accurately estimated that the diagnostic or prognostic efficacy of specific quantitative physiological parameters can be properly tested.

ACKNOWLEDGMENTS

Preliminary studies were carried out in the laboratory of Steve Blackband, Department of Neuroscience, University of Florida. I am grateful to Xiao Ping Zhu, Ka-Loh Li, and Alan Jackson, University of Manchester, for kindly providing example data, and to Keith St. Lawrence, Geoff Parker, and Stephen R. Williams for their insightful comments. The National Simulation Resource is supported by the NIH (RR-01243).

REFERENCES

1. Parker GJM, Tofts PS. Pharmacokinetic analysis of neoplasms using contrast-enhanced dynamic magnetic resonance imaging. Top Magn Reson Imaging 1999;10:130–143.
2. Fritz-Hansen T, Rostrup E, Sondergaard L, Ring PB, Amtorp O, Larsson HBW. Capillary transfer constant of Gd-DTPA in the myocardium at rest and during vasodilation assessed by MRI. Magn Reson Med 1998; 40:922–929.
3. Buckley DL, Drew PJ, Mussurakis S, Monson JRT, Horsman A. Microvessel density in invasive breast cancer assessed by dynamic Gd-DTPA enhanced MRI. J Magn Reson Imaging 1997;7:461–464.
4. van der Sanden BPJ, Rozijn TH, Rijken PFJW, Peters HPW, Heerschap A, van der Kogel AJ, Bovee WMMJ. Noninvasive assessment of the functional neovasculature in 9L-glioma growing in rat brain by dynamic H-1 magnetic resonance imaging of gadolinium uptake. J Cereb Blood Flow Metab 2000;20:861–870.
5. Larson KB, Markham J, Raichle ME. Tracer-kinetic models for measuring cerebral blood flow using externally detected radiotracers. J Cereb Blood Flow Metab 1987;7:443–463.
6. Henderson E, Rutt BK, Lee TY. Temporal sampling requirements for the tracer kinetics modeling of breast disease. Magn Reson Imaging 1998; 16:1057–1073.
7. Calamante F, Gadian DG, Connelly A. Delay and dispersion effects in dynamic susceptibility contrast MRI: simulations using singular value decomposition. Magn Reson Med 2000;44:464–473.
8. Ostergaard L, Chesler DA, Weisskoff RM, Sorensen AG, Rosen BR. Modeling cerebral blood flow and flow heterogeneity from magnetic resonance residue data. J Cereb Blood Flow Metab 1999;19:690–699.
9. Tofts PS, Kermode AG. Measurement of the blood-brain barrier permeability and leakage space using dynamic MR imaging. I. Fundamental concepts. Magn Reson Med 1991;17:357–367.
10. Parker GJM, Tanner SF, Leach MO. Pitfalls in the measurement of tissue permeability over short time-scales using a low temporal resolution blood input function. In: Proceedings of the 4th Annual Meeting of ISMRM, New York, 1996. p 1582.
11. Fritz-Hansen T, Rostrup E, Larsson HB, Sondergaard L, Ring P, Henriksen O. Measurement of the arterial concentration of Gd-DTPA using MRI: a step toward quantitative perfusion imaging. Magn Reson Med 1996;36:225–231.
12. Li K-L, Zhu XP, Waterton J, Jackson A. Improved 3D quantitative mapping of blood volume and endothelial permeability in brain tumors. J Magn Reson Imaging 2000;12:347–357.
13. Bassingthwaighte JB, Goresky CA. Modeling in the analysis of solute and water exchange in the microvasculature. In: Renkin EM, Michel CC, Geiger SR, editors. Handbook of physiology. Section 2. The cardiovascular system. Bethesda: American Physiological Society; 1984. p 549–626.
14. Kroll K, Wilke N, Jerosch-Herold M, Wang Y, Zhang Y, Bache RJ, Bassingthwaighte JB. Modeling regional myocardial flows from residue functions of an intravascular indicator. Am J Physiol 1996;271:H1643–H1655.
15. Buckley DL. Modelling contrast uptake by neoplasms using dynamic magnetic resonance imaging. Ph.D. thesis, University of Hull; 1996.
16. Jain RK. Determinants of tumor blood flow: a review. Cancer Res 1988;48:2641–2658.
17. Tofts PS. Modeling tracer kinetics in dynamic Gd-DTPA MR imaging. J Magn Reson Imaging 1997;7:91–101.
18. Kety SS. The theory and applications of the exchange of inert gas at the lungs and tissues. Pharmacol Rev 1951;3:1–41.
19. Larsson HBW, Stubgaard M, Frederiksen JL, Jensen M, Henriksen O, Paulson OB. Quantitation of blood-brain barrier defect by magnetic resonance imaging and gadolinium-DTPA in patients with multiple sclerosis and brain tumors. Magn Reson Med 1990;16:117–131.
20. Tofts PS, Brix G, Buckley DL, Evelhoch JL, Henderson E, Knopp MV, Larsson HB, Lee TY, Mayr NA, Parker GJ, Port RE, Taylor J, Weisskoff RM. Estimating kinetic parameters from dynamic contrast-enhanced T_1-weighted MRI of a diffusable tracer: standardized quantities and symbols. J Magn Reson Imaging 1999;10:223–232.
21. St. Lawrence KS, Lee TY. An adiabatic approximation to the tissue homogeneity model for water exchange in the brain. I. Theoretical derivation. J Cereb Blood Flow Metab 1998;18:1365–1377.
22. Henderson E, Sykes J, Drost D, Weinmann HJ, Rutt BK, Lee TY. Simultaneous MRI measurement of blood flow, blood volume, and capillary permeability in mammary tumors using two different contrast agents. J Magn Reson Imaging 2000;12:991–1003.
23. Jerosch-Herold M, Wilke N, Wang Y, Gong GR, Mansoor AM, Huang H, Gurchumelidze S, Stillman AE. Direct comparison of an intravascular and an extracellular contrast agent for quantification of myocardial perfusion. Int J Card Imaging 1999;15:453–464.
24. Mussurakis S, Buckley DL, Drew PJ, Fox JN, Carleton PJ, Turnbull LW, Horsman A. Dynamic MR imaging of the breast combined with analysis of contrast agent kinetics in the differentiation of primary breast tumours. Clin Radiol 1997;52:516–526.